OPEN ACCESS

Klimarealistene
Vollsveien 109
1358 Jar, Norway
ISSN: 2703-9072

Correspondence:
dk@itia.ntua.gr

Vol. 4.2 (2024)
pp. 36-78

Relative importance of carbon dioxide and water in the greenhouse effect: Does the tail wag the dog?

Demetris Koutsoyiannis

Department of Water Resources and Environmental Engineering, School of Civil Engineering, National Technical University of Athens, Zographou, Greece

Abstract

Using a detailed atmospheric radiative transfer model, we derive macroscopic relationships of downwelling and outgoing longwave radiation which enable determining the partial derivatives thereof with respect to the explanatory variables that represent the greenhouse gases. We validate these macroscopic relationships using empirical formulae based on downwelling radiation data, commonly used in hydrology, and satellite data for the outgoing radiation. We use the relationships and their partial derivatives to infer the relative importance of carbon dioxide and water vapour in the greenhouse effect. The results show that the contribution of the former is 4% – 5%, while water and clouds dominate with a contribution of 87% – 95%. The minor effect of carbon dioxide is confirmed by the small, non-discernible effect of the recent escalation of atmospheric CO_2 concentration from 300 to 420 ppm. This effect is quantified at 0.5% for both downwelling and outgoing radiation. Water and clouds also perform other important functions in climate, such as regulating heat storage and albedo, as well as cooling the Earth's surface through latent heat transfer, contributing 50%. By confirming the major role of water on climate, these results suggest that hydrology should have a more prominent and more active role in climate research.

Keywords: Greenhouse effect; longwave radiation; water vapour; carbon dioxide; evaporation radiative forcing

Submitted 2024-09-22, Accepted 2024-10-28. https://doi.org/10.53234/scc202411/01

A good rule of thumb to keep in mind is that anything that calls itself 'science' probably isn't.

J.R. Searle (1984)

1. Introduction

A notable feature of the current period is that the classical value of science as the pursuit of the truth, independently of other interests, is gradually being abandoned (Koutsoyiannis and Mamassis, 2021). People pride themselves on being scientists and activists at the same time (Koutsoyiannis, 2020b), while calls for political actions to "save the planet", including enhanced global governance, are published even in scientific journals (e.g. Biermann et al., 2012). While common perception promotes the idea of science-based policies and politics, the reality is the exact opposite, i.e., politics-based science. For it is self-evident that by mixing science and politics the end product is politics. A relevant example is provided by the high-profile journal *Nature*, which declares that it is "committed to supporting the research enterprise"[1], but admits being involved in politics and proclaims that this is the right thing (Howe, 2020; Nature Editorial, 2023),

[1] Nature, Editorial Values Statement, https://www.nature.com/nature/editorial-values-statement (accessed 27 March 2024).

even though it is recognized that this affects scientific credibility and causes loss of confidence in science (Lupia, 2023; Zhang, 2023). Another relevant example is the campaign of a famous learned society, the American Geophysical Union (AGU), related to the USA 2024 election.[2]

It is thus natural to wonder if articles published in scientific journals promote the truth or political aims, perhaps hiding or distorting the truth, and even reversing cause and effect (Koutsoyiannis, 2021; Koutsoyiannis et al. 2022a,b, 2023). Gradually, by repetition and accumulation, distorted information becomes dominant among the scientific community and the public. In contrast, studies providing information different from the dominant tend to be suppressed (the current study serves as an example—see Supplementary Information).

Seeking truth may have been even more difficult due to a recent development, the appearance of artificial intelligence (AI) bots, which certainly affects common opinion, as well as scientific perception and advancement. Assuming that AI bots more or less reflect the common perception in the scientific community and the general public, Microsoft Bing's chatbot was asked the following question:

> *Which gas determines the greenhouse effect on Earth?*

The bot provided the following answer[3]:

> *The greenhouse effect is the process through which heat is trapped near Earth's surface by substances known as 'greenhouse gases.' These gases consist of carbon dioxide, methane, ozone, nitrous oxide, chlorofluorocarbons, and water vapor. Water vapor, which reacts to temperature changes, is referred to as a 'feedback', because it amplifies the effect of forces that initially caused the warming. Scientists have determined that carbon dioxide plays a crucial role in maintaining the stability of Earth's atmosphere. If carbon dioxide were removed, the terrestrial greenhouse effect would collapse, and Earth's surface temperature would drop significantly, by approximately 33°C (59°F).*

A literature search reveals that the chatbot essentially (and selectively) reproduces the following statements by Lacis et al. (2010), in which the atmospheric CO_2 is presented as the principal control knob governing Earth's temperature:

> *Noncondensing greenhouse gases, which account for 25% of the total terrestrial greenhouse effect, thus serve to provide the stable temperature structure that sustains the current levels of atmospheric water vapor and clouds via feedback processes that account for the remaining 75% of the greenhouse effect. Without the radiative forcing supplied by CO_2 and the other noncondensing greenhouse gases, the terrestrial greenhouse would collapse, plunging the global climate into an icebound Earth state.* […]
>
> *If the global atmospheric temperatures were to fall to as low as $T_S = T_E$* [where $T_E = 255$ K is the global mean effective temperature] *the Clausius-Clapeyron relation would imply that the sustainable amount of atmospheric water vapor would become less than 10% of the current atmospheric value.*

Interestingly, while Lacis et al. recognize a high contribution of water vapour and clouds, they regard them as results of feedback processes of the CO_2 control knob. Moreover, the estimate of 75% they provide is too low, as we will see below.

On the other hand, Koutsoyiannis and Vournas (2024) recently examined longwave radiation observations extending over a century-long period and found that the observed increase of the atmospheric carbon dioxide concentration ([CO_2]; from 300 to 420 ppm) has not altered, in a discernible manner, the greenhouse effect, which remains dominated by the quantity of water vapour in the atmosphere. Naturally, given the uproar about the enhancement of the greenhouse effect

[2] AGU, This November Stand Up For Science, https://sciencevotesthefuture.org/ (accessed 27 Oct. 2024).

[3] It also provided references to: climate.nasa.gov; britannica.com; britannica.com

due to human emissions by fossil fuel combustion, this finding appeared surprising to many. Some (including a knowledgeable reviewer of Koutsoyiannis and Vournas, 2024) postulated that this would be expected for the downwelling longwave (LW) radiation flux, which was the subject of Koutsoyiannis and Vournas (2024), but this would not be the case for the outgoing radiation, where the effect of [CO_2] increase would be substantial. However, no long data series exist to verify such a conjecture and hence this question was not investigated in Koutsoyiannis and Vournas (2024), whose scope was to make inference based on data.

Hence the following research questions are raised:

1. Are Lacis et al. right about the importance of CO_2 in the greenhouse effect, and is it meaningful to state that without it the terrestrial greenhouse would collapse? Or is the effect of CO_2 negligible as Koutsoyiannis and Vournas (2024) claimed, and that of H_2O dominant?
2. Is the role of H_2O as a greenhouse gas limited to the downwelling LW flux or does it extend also to the outgoing LW flux?

We will examine these questions below, noting that the first one refers to a fictitious case (removal of atmospheric CO_2) for which no empirical data can exist. Rather, paleoclimatic studies and geological facts suggest that CO_2 existed, mostly in much higher concentrations than today, in most periods of Earth's history (see its evolution during the Phanerozoic in Koutsoyiannis, 2024a), and also before oxygen appeared in the atmosphere. Also, the second question cannot be studied on a purely empirical basis, as no long-term data exist. For systematic satellite measurements of outgoing LW flux have only been made in the 21st century. Therefore, to study these questions we need to resort to theoretical arguments and analyses. We will do this by applying the established greenhouse theory and by enrolling standard models, without considering doubts that have been cast on the validity of the theory or alternative hypotheses (e.g. Nikolov and Zeller, 2017, Miskolczi, 2023). In applying this theory, we will follow a macroscopic approach, without discussing the details of the physical processes related to radiation and the physical mechanisms thereof. The reader interested in the latter may find relevant critical discussions in Harde (2013, 2014, 2017) and Clark (2024).

Human CO_2 emissions are 4% of the total (Koutsoyiannis et al., 2023) but there are also human H_2O emissions over the terrestrial part of Earth of a comparable percentage (Peachey, 2006; Sherwood et al., 2018; Li et al., 2024). Specifically, according to Koutsoyiannis (2020a) the quantity of evaporation and transpiration over land is 91 400 km^3/year. According to the Food and Agriculture Organization of the United Nations[4], the human water withdrawal in 2010, including the evaporation from reservoirs, was 4 300 km^3/year, of which 69% and 19% were for agricultural and industrial use, respectively. Considering the fact that almost all agricultural and a large part of industrial water are evaporated, and taking into account the increasing trend in water withdrawal, with simple calculations we may conclude that the current human addition to the natural water cycle over land is about 4%. One could speculate that each of these 4% additions might influence the climate to a degree comparable to that percentage, but the reasons that only the influence of CO_2 is investigated and highlighted by the scientific community, being regarded as a control knob of climate (even though H_2O is much stronger as a greenhouse gas) are not scientific.

We may note, though, that the percentage of human H_2O emissions becomes much lower, of the order of 1%, if we also consider the evaporation over oceans, where there is no human intervention. However, it appears reasonable for this estimate of human water emissions to consider only the terrestrial part of Earth, because of the high local variability and the small residence time of atmospheric water. Indeed, the mean residence time of atmospheric water is a few days (specifically, 12 250 km^3 / (522 700 km^3/year) = 0.023 years = 8.6 d, where the total volume of liquid

[4] Water use – AQUASTAT - FAO's Global Information System on Water and Agriculture https://www.fao.org/aquastat/en/overview/methodology/water-use (accessed 19 February 2024).

water in the atmosphere, 12 250 km^3, was taken as the average atmospheric water content, 24.0 kg/m^3, as estimated from the ERA5 Reanalysis (see explanation about ERA5 in Section 3) over the globe for the period 1950-2023, while the atmospheric inflow volume of water, 522 700 km^3/year, was taken from Koutsoyiannis, 2020a). In contrast, CO_2 is well mixed as it has a much higher residence time, of a few years (specifically, 4 years according to Koutsoyiannis, 2024b)[5].

The thesis expressed in this paper is that none of these anthropogenic additions to the hydrological and carbon cycle drives climate. On the other hand, both H_2O and CO_2 are important elements of climate and their quantities and fluxes are determined by natural processes, with the human factor being rather negligible. Both are elixirs of life and in this respect, they act complementary to each other. Thus, it may be pointless to compare them to each other. Yet this comparison is the main focus of this paper, as lately, the scientific efforts to study each of them have been inversely proportional to their respective importance.

By its definition by UNESCO (1964), hydrology is the science that deals with the waters of the Earth, and its domain covers the entire history of the cycle of water on the Earth. Water is a critical element of life and of climate as well. While climate has become a hot topic and its research a top priority, it is odd that hydrology has lost importance, as evident from the abundance of papers examining climate change impacts on water and applying model projections for the future based on CO_2 emission scenarios. This misses the fact that water is the key element on Earth in driving climate and that the hydrological cycle is self-ruling rather than a feedback or impact of another cycle—namely the carbon cycle, which has also been downgraded to an issue governed by human carbon emissions (the 4% of the total).

By emphasizing the relative importance of water in climate, in comparison to carbon dioxide, this paper tries to show that the picture of Earth's climatic system may have been distorted and to reinstate the importance of water and hydrology (and its branch of hydrometeorology) in climate. The paper is made as a stand-alone and therefore it includes a synopsis of the related theoretical concepts and a model (Section 2 and Appendices A and B). Its foundation is not only theoretical but also empirical, utilizing observed data (Section 3). By combining the model and data, it derives simple macroscopical empirical relationships representing the greenhouse effect as accurately as the detailed model whose results are based upon (Section 4). These relationships are tested against observational data (Section 5) and their simple and analytical expressions, which enable extraction of partial derivatives, allow the comparison of the effect of water relative to other greenhouse gases (Section 6). The findings are put in a more general context (Section 7) and allow drawing relevant conclusions (Section 8).

2. Theoretical Background

The typical quantification of the abundance of a specific gas X in a gas mixture is given by its concentration, defined in terms of mole fraction as:

$$[X] := \frac{n_X}{n_{\mathrm{TOT}}} = \frac{N_X}{N_{\mathrm{TOT}}} \tag{1}$$

where n_X and n_{TOT} are the numbers of moles of the gas X contained in a specified volume and the total amount of moles of all constituents in the same volume, and N_X and N_{TOT} are the respective number of molecules; note that $n_X = N_X/N_A$, where $N_\mathrm{A} = 6.022\times10^{23}$ mol^{-1} is the Avogadro constant (and likewise for n_{TOT}). Additional metrics are discussed in Appendix A. The simple metric in Equation (1) is sufficient to quantify noncondensing greenhouse gases, such as CO_2,

[5] This can also be verified by estimates of the Intergovernmental Panel on Climate Change (IPCC) report (Masson-Delmotte et al., 2021), namely its figure 5.12. Specifically, we obtain 870 Gt / (226.9 Gt/year) = 3.8 years, where the total mass of atmospheric CO_2, 870 Gt was taken from the IPCC report, while the atmospheric inflow mass, 226.9 Gt/year, is taken from Koutsoyiannis et al. (2023).

with concentration (denoted as [CO_2]) only slightly varying geographically on long time scales. However, in the case of water vapour, its concentration varies substantially in space and time, and its vapour pressure, e_a, has a thermodynamic upper limit, the saturation water vapour pressure, which is a function, $e(T_a)$, of temperature, T_a. Therefore, we need a more sophisticated framework of quantification, which is again summarized in Appendix A.

Accordingly, the quantification of the greenhouse effect due to the presence of water vapour in the atmosphere is more demanding than that due to CO_2. However, there is a very rich experience for this quantification as it has been necessary for routine calculations of evapotranspiration, which represents a substantial component of the hydrological balance—and also the most intractable and difficult to measure. Evaporation calculations are also most essential for agricultural irrigation practice. The details of this quantification are presented in Appendix A. The related macroscopic formulae for the clear-sky LW radiation flux are based on two variables, the temperature, T_a, and the water vapour pressure, e_a, and a single value of each of them near the Earth's surface. This clearly reflects the fact that it is the water vapour that determines the greenhouse effect on Earth's atmosphere, contrary to the public perception that this is CO_2. Remarkably, the latter does not appear at all in the related formulae. Koutsoyiannis and Vournas (2024) demonstrated that, indeed, there is no need to involve [CO_2] in these calculations as the observations in a century-long period, in which the rise of [CO_2] was substantial, there was no discernible effect on the greenhouse effect.

However, for reasons explained in the Introduction, we seek to quantify the contribution of CO_2 to the greenhouse effect and compare it to that of water vapour. In this, we need to enrol detailed modelling of the spectroscopic properties of the atmosphere. Also, while the formulae of Appendix A are useful for the downwelling radiation, they do not quantify the outgoing radiation at the top of the atmosphere (TOA). For those tasks, we may use detailed spectroscopic models.

There are several databases of spectroscopic parameters and codes that perform detailed modelling of radiation in the atmosphere. Of these, here we use the MODerate resolution atmospheric TRANsmission model, or MODTRAN (Berk et al. (1987, 2008, 2014), which has been extensively validated in its over 30-year history, and serves as a community standard atmospheric band model. It simulates the emission and absorption of infrared radiation in the atmosphere, and particularly the effect of wavelength-selective greenhouse gases on Earth's LW radiation flux.

The specific implementation used is that of the University of Chicago, readily provided as an interactive web application[6]. The application is based on five different locality cases, which differ most significantly in their temperature, water vapour and ozone profiles, as specified in Appendix B. The application offers default values of several characteristics for each locality profile but also allows modifying these values (e.g., by offsetting temperature and holding fixed either the water vapour pressure or the relative humidity, or by multiplying the water vapour scale by a constant). Finally, in addition to the clear-sky conditions, it enables the use of several different cloud types, as will be described in Section 4.2.

A typical graphical output of the MODTRAN application is seen in Figure 1. This is for the standard tropical atmospheric profile, also in comparison to the case that the standard [CO_2] of 400 ppm is replaced by that of 800 ppm, where the difference is difficult to discern. The effect of the different greenhouse gases is also marked in the figure. It is clear that the effect of H_2O dominates, particularly in the downwelling radiation. Note that, according to Clark (2024, Fig. 19), 95% of the downwelling radiation originates from within the first 2 km layer and approximately half originates from the first 100 m layer above the surface.

As the MODTRAN web application only models the longwave radiation, in a case where the

[6] MODTRAN Demo, http://modtran.spectral.com/modtran_home (accessed 19 February 2024). Additional web applications can be found in other sites, such as MODTRAN Infrared Light in the Atmosphere. https://climatemodels.uchicago.edu/modtran/ (accessed 19 February 2024).

shortwave (SW) radiation was needed in this study, this was estimated by another model, RRTM (standing for Earth's Energy Budget), again available as a web application by the University of Chicago[7]. This simulates both LW and SW radiation fluxes, both upward and downward.

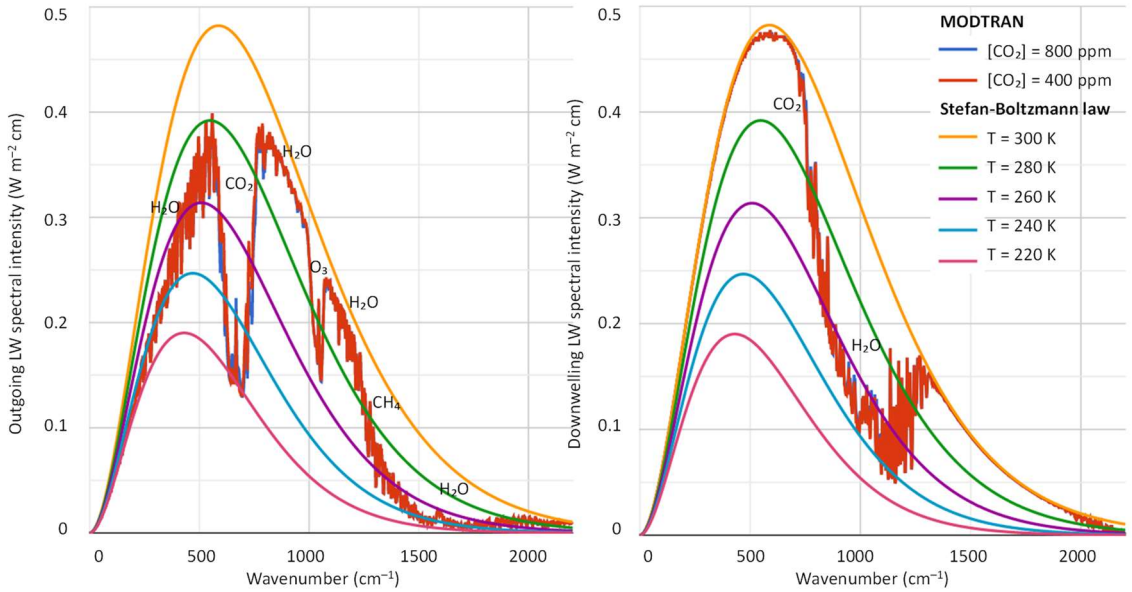

*Figure 1: Output of the MODTRAN model for the standard, cloud free, tropical atmospheric profile, in comparison to the case that the standard [CO_2] of 400 ppm is replaced by that of 800 ppm: (**left**) outgoing radiation corresponding to the level of 100 km above the ground; (**right**) downwelling radiation at zero level. The ground temperature is 299.7 K (26.55 °C) and the total outgoing and downwelling LW flux are, respectively, 298.52 and 369.26 W/m² for [CO_2] = 400 ppm, and 295.129 and 371.14 W/m² for [CO_2] = 800 ppm (differences: –3.36 and 1.88 W/m²). The gases mostly affecting LW radiation are noted for the respective wavenumbers. Graph generated from https://climatemodels.uchicago.edu/modtran/.*

3. Data

To compare MODTRAN results to observed radiation profiles in the atmosphere, we need radiosonde data. While radiosondes are routinely made in several hundreds of sites across the world, they typically measure temperature, humidity, pressure and wind. Radiation radiosonde measurements are rare, yet it is useful to make at least a single comparison to get a general idea. Here we use a couple of radiosondes from a day and a night flight on 23 September 2011, in cloud-free conditions, at the aerological station in Payerne, Switzerland (6.9440° E, 46.8130°, +491 m a.s.l.). In these, in-situ measurements of downward and upward radiation fluxes were taken through the troposphere and into the stratosphere, exceeding 32 km of altitude. They were presented by Philipona et al. (2012) in graphical form in their figure 2, which was digitized here to recover the measurements.

For the downwelling LW radiation flux, there have been numerous measurements at specific sites for more than a century, which are presented in Koutsoyiannis and Vournas (2024). These were the basis for the derivation of the empirical or semiempirical formulae for the calculation of the downwelling radiation flux, discussed in Section 2 and Appendix A. Considering that these formulae reflect the data that they were based upon, here we use the formulae, instead of the data, for comparisons with MODTRAN.

Information for the radiation fluxes at the top of the atmosphere (TOA), including the LW fluxes, are provided by satellite instruments. These are available only for the 21st century from the

[7] RRTM Earth's Energy Budget, https://climatemodels.uchicago.edu/rrtm/ (accessed 19 February 2024).

ongoing project Clouds and the Earth's Radiant Energy System (CERES), a part of NASA's Earth Observing System, designed to measure both solar-reflected and Earth-emitted radiation from the TOA (in CERES defined at the altitude of 20 km) to the surface.

The specific product used here is the CERES SSF1deg monthly averaged TOA LW radiative fluxes at a 1°-regional grid, constant-meteorology-temporally-interpolated (Wielicki et al., 1996; Doelling et al., 2013, 2016). The TOA fluxes are provided for clear-sky and all-sky conditions. Both these observational data are available online[8] and were retrieved here for their entire time span of complete years, i.e., from January 2001 to December 2022 from the Terra platform. The same CERES product provides information on clouds, which was also retrieved (monthly averaged for both day and night).

In addition, the CERES project provides LW fluxes for the surface, both downwelling and upgoing, through the product CERES_EBAF_Ed4.2, where EBAF stands for "Energy Balanced and Filled" (Kato et al., 2018; Loeb et al., 2018). However, these are computed gridded values rather than observational data. They are publicly available[9] and were also retrieved here.

The CERES data are associated with considerable uncertainties. According to CERES (2023), the combined regional all-sky LW flux uncertainty is 2.4 W/m² and the daily regional all-sky LW diurnal uncertainty is 8 W/m². According to CERES (2021, Table 6.1), the uncertainties in the 1°×1° regional monthly TOA fluxes are 4.6 W/m² for clear sky and 2.5 W/m² for all sky. In addition, as also noted in CERES (2021), with the most recent CERES instrument calibration improvements, there still is a net imbalance of ~4.3 W/m², much larger than the expected observed ocean heating rate which CERES assumes to be ~0.71 W/m². The latter value is not far from that of Trenberth et al. (2009), who give the net absorbed energy at 0.9 W/m^2. However, according to the calculations by Koutsoyiannis (2021), the latter imbalance value, again inferred from ocean heating data, is lower, 0.37 W/m². The EBAF dataset adjusts the observations in view of the above inconsistencies. All this information suggests that the observational uncertainties are far too high to allow calculations of Earth's imbalance and of temporal climatic changes, yet they are quite useful for the very scope of this study, which is not related to energy flux imbalances.

Additional atmospheric variables used here, namely temperature and water vapour pressure, are taken from the ERA5 and NCEP/NCAR Reanalyses at a monthly scale. ERA5 stands for the fifth-generation atmospheric reanalysis of the European Centre for Medium-Range Weather Forecasts (ECMWF; ECMWF ReAnalysis). Its data are publicly available for the period 1940 onwards at a spatial resolution of 0.5°. NCEP/NCAR stands for Reanalysis 1 by the National Centers for Environmental Prediction (NCEP) and the National Center for Atmospheric Research (NCAR). Its data are publicly available from 1948 to the present at a horizontal resolution of 1.88° (~ 210 km). Both data sets can be retrieved from the Climexp platform[10] and from the Physical Sciences Laboratory platform of the US National Oceanic and Atmospheric Administration (NOAA)[11]. Finally [CO_2] data were retrieved for the most well-known station, Mauna Loa, again from the Climexp platform.

The gridded CERES SSF1deg TOA LW data are presented in Figure 2, averaged over the period of observations. The cloud information (cloud area fraction) of the same data product is shown in Figure 3. The zonal distribution of the LW radiation data are shown in Figure 4, along with that of temperature, and, as expected, the distributions of the two variables are similar.

---

[8] CERES_SSF1deg_Ed4.1 Subsetting and Browsing, https://ceres-tool.larc.nasa.gov/ord-tool/jsp/SSF1degEd41Selection.jsp (accessed 19 February 2024).

[9] CERES_EBAF_Ed4.2 Subsetting and Browsing, https://ceres-tool.larc.nasa.gov/ord-tool/jsp/EBAF42Selection.jsp (accessed 19 February 2024).

[10] Climate Explorer: https://climexp.knmi.nl/ (last access: 19 February 2024).

[11] WRIT: Monthly Timeseries: NOAA Physical Sciences Laboratory, https://psl.noaa.gov/cgi-bin/data/atmoswrit/timeseries.pl (accessed 19 February 2024).

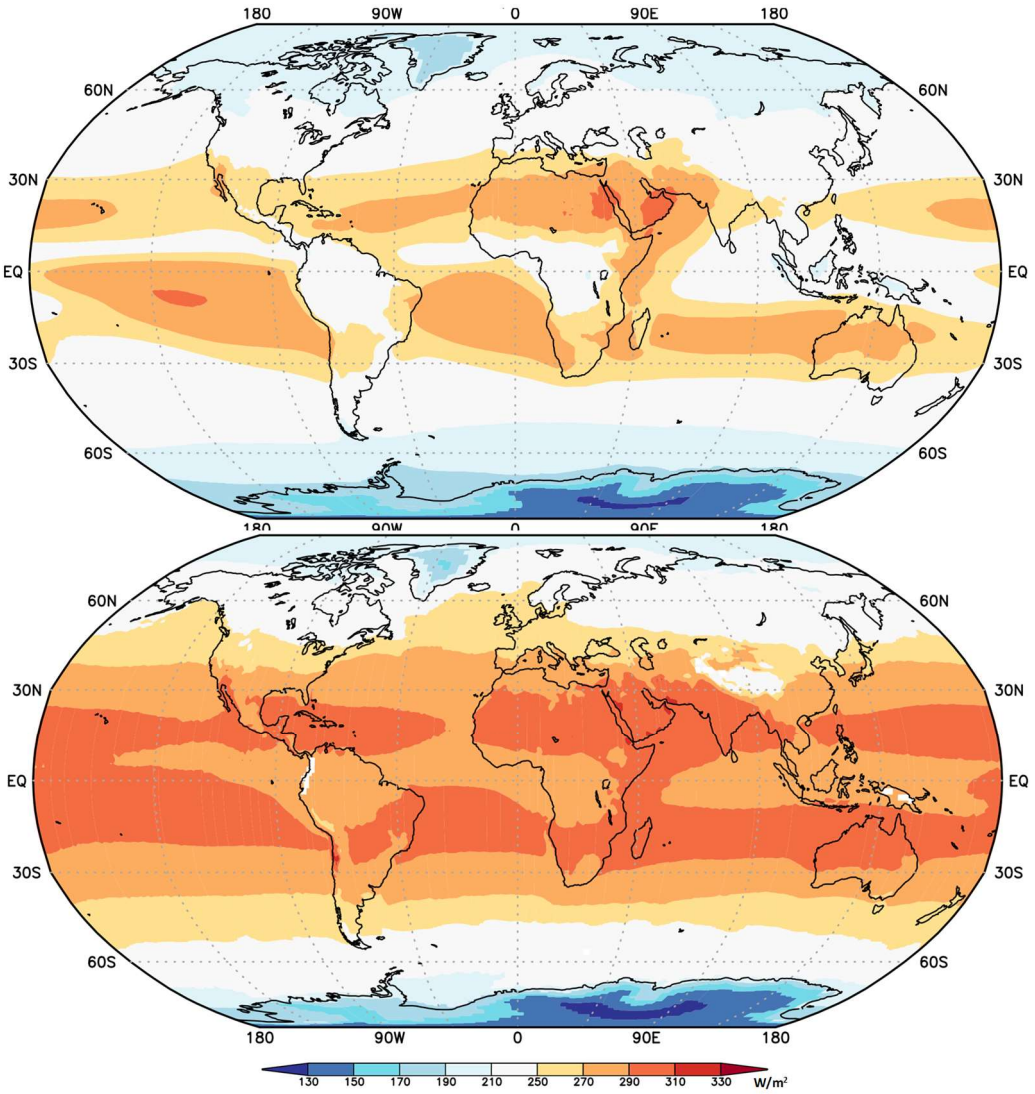

*Figure 2: Geographical distribution of outgoing LW radiation averaged over the period of 2000 – 2022 as given by the CERES data: (**upper**) all sky; (**lower**) clear sky. Data retrieved from [https://ceres-tool.larc.nasa.gov/ord-tool/jsp/SSF1degEd41Selection.jsp;](https://ceres-tool.larc.nasa.gov/ord-tool/jsp/SSF1degEd41Selection.jsp) graph generated by https://climexp.knmi.nl.*

Figure 5, constructed from the data of Figure 4, shows that the torrid zone (between 23.4° S and 23.4° N) contributes 43% of Earth's outgoing LW radiation flux, and together with the two temperate zones (between 23.4° and 66.6° S and N) radiates 94% of the total, leaving only 6% for the frigid zones (between 66.6° and 90° S and N).

Figure 6 better depicts the relationship of outgoing LW radiation flux and surface temperature, for each month of the 22 years of data availability separately, but areally averaged over geographical zones of 15° latitude. This graph allows important observations. First, the individual monthly values align very well with the average zonal distribution. Second, the relationship between temperature and outgoing LW radiation appears to be linear at most part of the graph. One would expect a 4th-power relationship, based on the Stefan-Boltzmann law (see Appendix A, Equation (A9)), but clearly this is not the case. The deviation has been explained as an emergent property of an atmosphere whose greenhouse effect is dominated by a condensable gas, namely water vapour (Koll and Cronin, 2018). Third, at the high end of temperature variation, around 300 K, there appears a stagnancy, or even regression of radiation with respect to temperature. This behaviour is observed in the tropics, where the maximum ocean surface temperature does not exceed 300 K. Evaporation, tropical clouds and thunderstorms actively regulate the temperature in this area blocking further temperature rise (Eschenbach, 2010; Clark, 2013a,b).

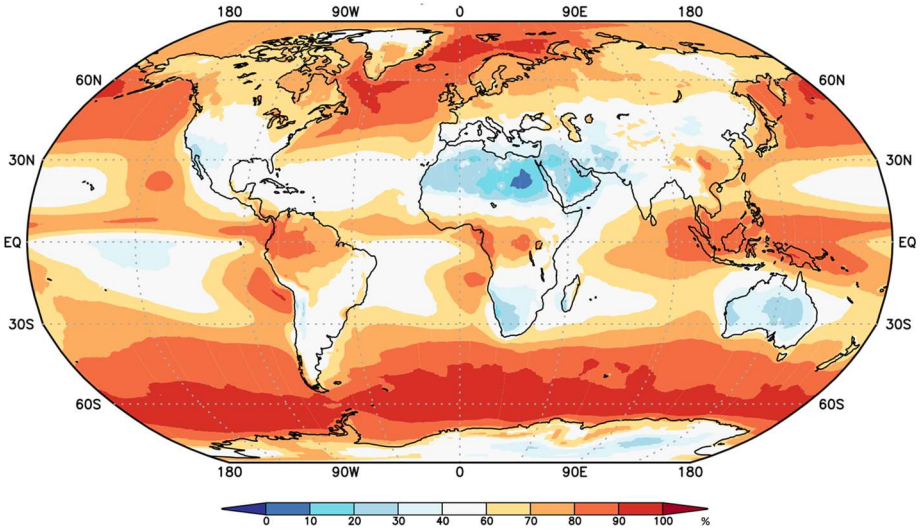

Figure 3: Geographical distribution of cloud area fraction averaged over the period of 2000 – 2022 as given by the CERES data. Data source and graph generation as in Figure 2.

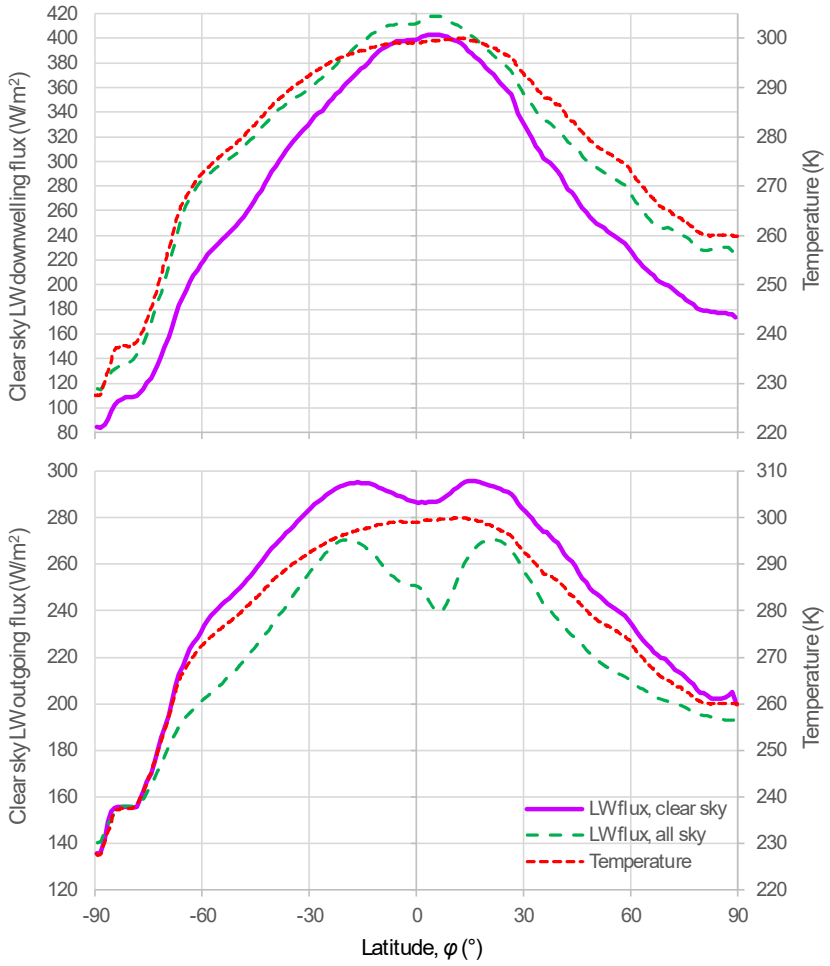

*Figure 4: Zonal distribution of LW radiation averaged from 2000 to 2022 as given by the CERES data: **(upper)** downwelling; **(lower)** outgoing; the temperature zonal distribution, as given by ERA5 Reanalysis is also plotted. Radiation data retrieved from https://ceres-tool.larc.nasa.gov/ord-tool/jsp/SSF1degEd41Selection.jsp for outgoing radiation and https://ceres-tool.larc.nasa.gov/ord-tool/jsp/EBAF42Selection.jsp for downwelling radiation; temperature data from ERA5 Reanalysis retrieved from https://climexp.knmi.nl.*

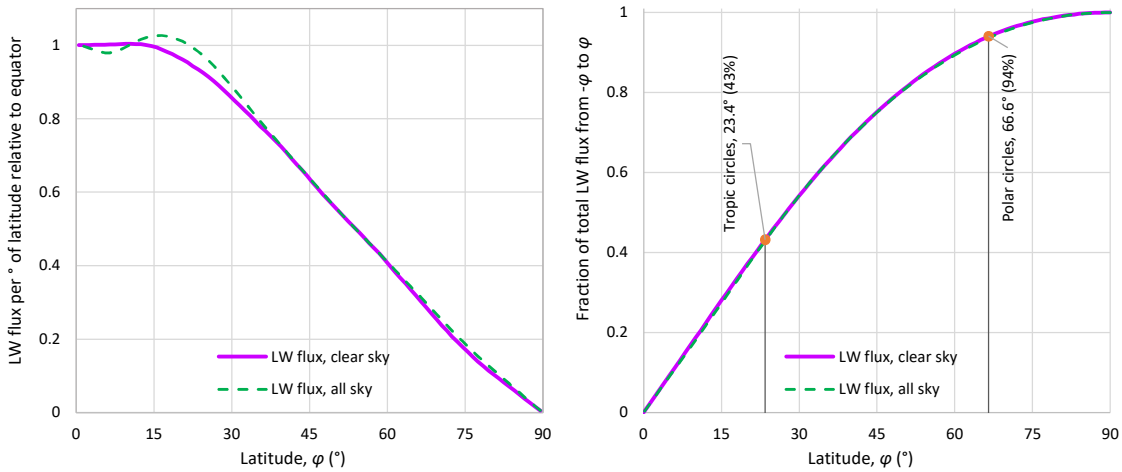

*Figure 5: Graphical depictions of the relative intensity of outgoing LW radiation averaged over the period of 2000 – 2022 as given by the CERES data, as a function of the latitude; (**left**) ratio of intensity at latitude φ (average for S and N) to that at the equator; (**right**) cumulative flux between latitudes φ S and φ N to the total outgoing radiation.*

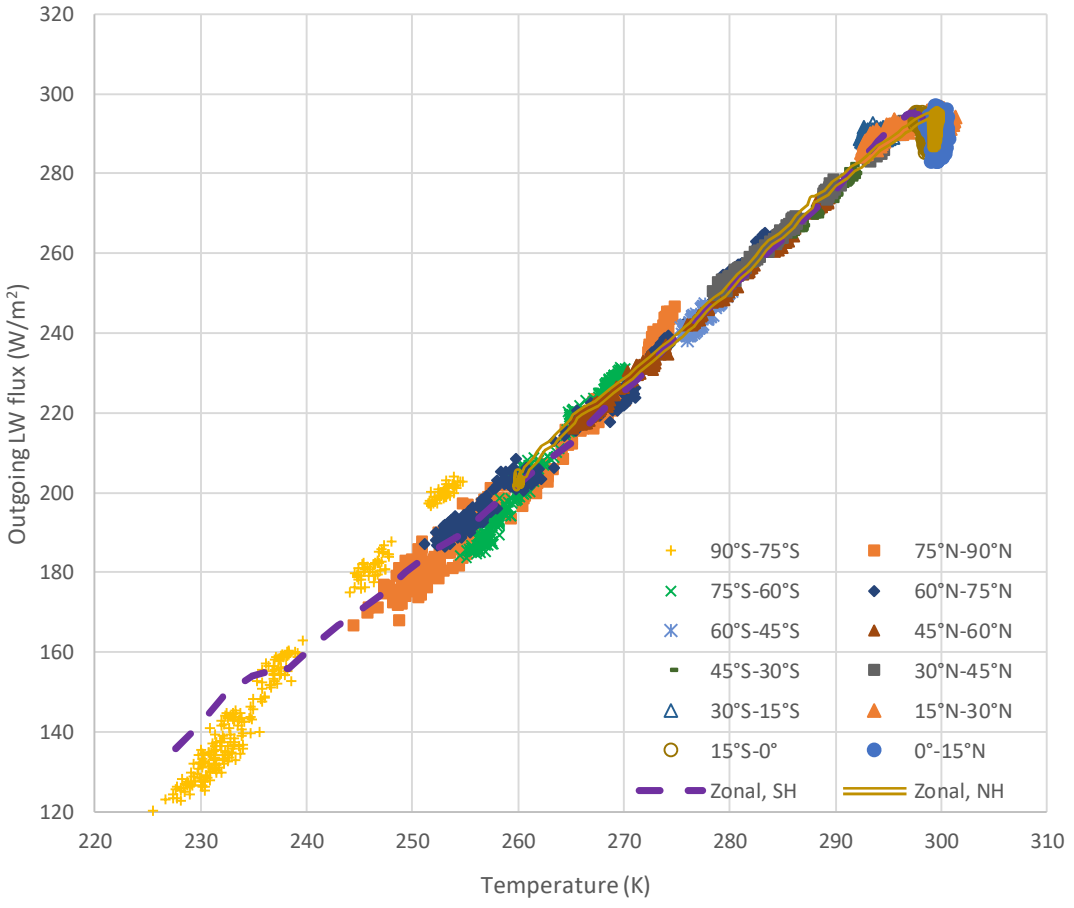

Figure 6: Depiction of monthly variability of outgoing LW radiation, as given by the CERES data; each point is the monthly value, spatially averaged over a geographical zone of 15° latitude, during the period of 2000 – 2022; the zonal distributions (temporal averages for the entire period as in Figure 4) are also shown for each hemisphere (SH and NH).

4. Macroscopic Relationships

4.1 Clear-sky Relationships

Faithful to Dooge's (1986) spirit of "looking for hydrologic laws", i.e., simple macroscopic laws for phenomena whose details are complex, this section tries to establish relationships between the downwelling and outgoing LW radiation fluxes with the variables that influence them, namely, temperature, water vapour pressure, carbon dioxide concentration and cloudiness. To this aim, it primarily uses MODTRAN outputs and also cloudiness information.

A series of systematic MODTRAN runs around the values of the standard tropical profile, i.e., $[CO_2]$ = 400 ppm and for surface T = 299.7 K and e_a = 19 hPa, with ranges of 200 – 800 ppm for $[CO_2]$, ±2 K for T and ±10% for e_a, gave the results shown in contour graphs in Figure 7 for the downwelling LW flux and in Figure 8 for the outgoing flux. Both figures suggest that the relationships among the involved variables are simple and that macroscopic representations are possible. Figure 7 shows a linear effect of e_a and a logarithmic one of $[CO_2]$ on the variation of the downwelling LW flux. In addition, it shows that a ±10% change in e_a has a larger effect than a doubling or halving of $[CO_2]$. Similar are the results of Figure 8, but with smaller differences in the effects of the two factors.

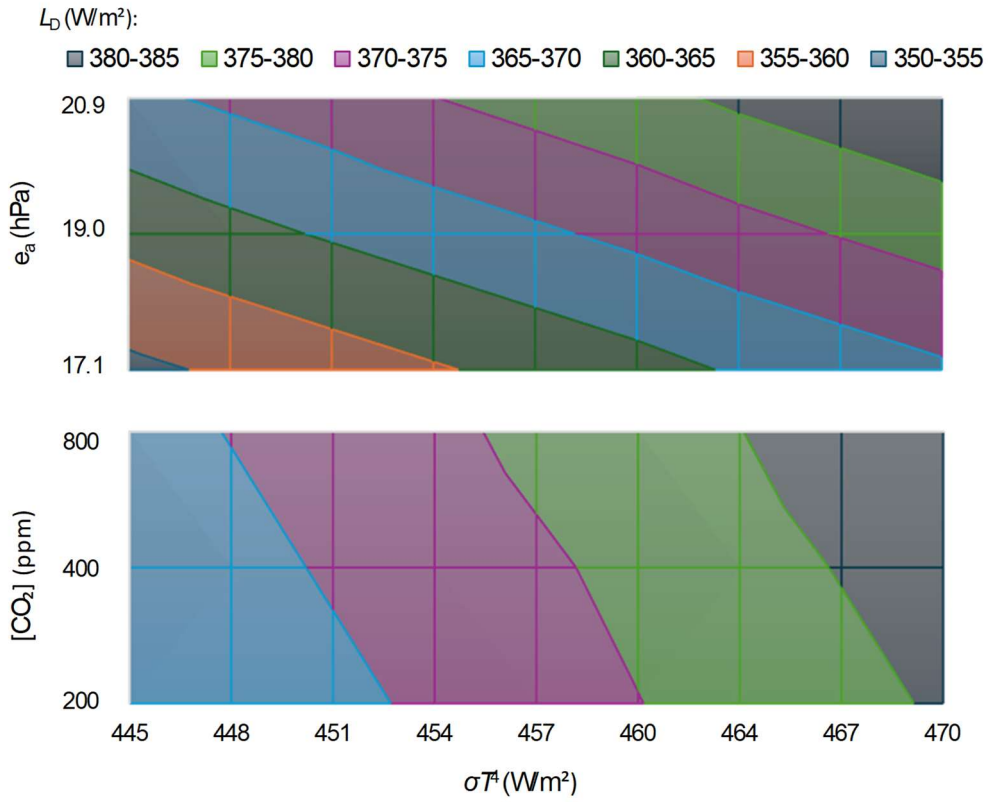

*Figure 7: Changes in the downwelling LW radiation, L_D, as calculated by MODTRAN, due to changes in temperature (converted to blackbody radiation, σT^4), and (**upper**) water vapour pressure (e_a) and (**lower**) carbon dioxide concentration ($[CO_2]$). The calculations were made for the tropical profile, no clouds and default other settings. For the upper graph it was assumed $[CO_2]$ = 400 ppm and for the lower graph e_a = 19 hPa. Notice that the scale of the vertical axis is linear in the upper graph (with range ±10% of the central value) and logarithmic in the lower graph (with range from half to twice the central value).*

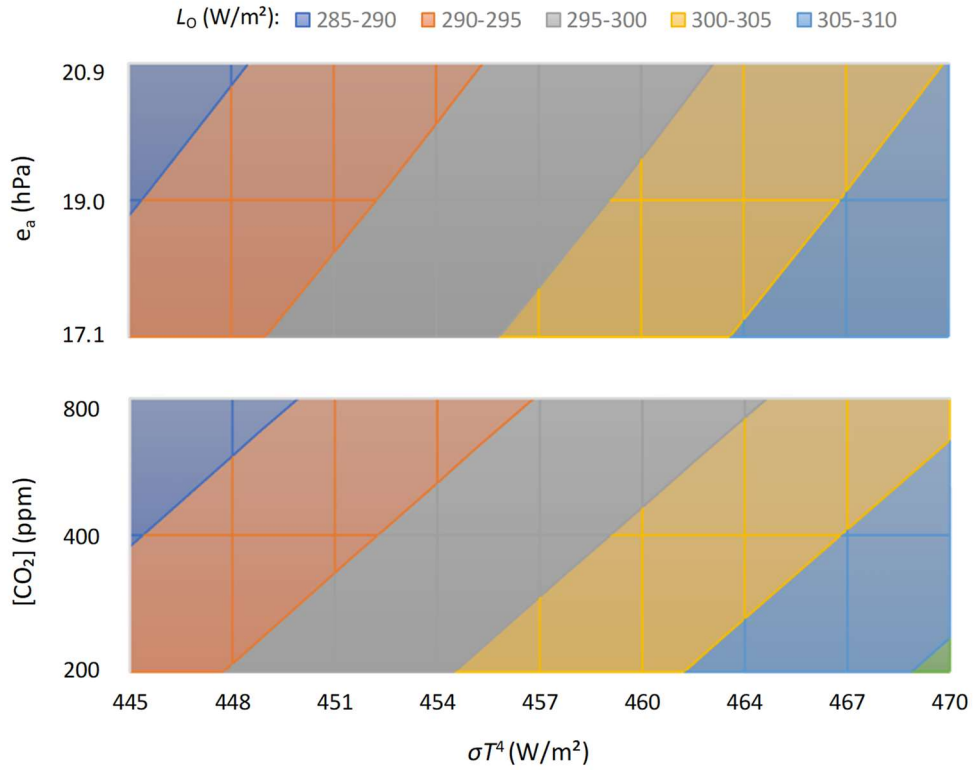

Figure 8: As in Figure 7 but for the outgoing LW radiation, L_O.

Based on these preliminary results, several mathematical expressions were formulated and fitted. The following equation was found to be the best for both the downwelling and outgoing flux, L_D and L_O, respectively:

$$L_{\mathrm{D,O}} = L^* \left(1 + \left(\frac{T}{T^*}\right)^{\eta_T} \pm \left(\frac{e_\mathrm{a}}{e_\mathrm{a}^*}\right)^{\eta_e}\right)\left(1 \pm a_{\mathrm{CO_2}} \ln\frac{[\mathrm{CO_2}]}{[\mathrm{CO_2}]_0}\right)(1 \pm a_C C) \qquad (2)$$

with $[\mathrm{CO_2}]_0$ = 400 ppm. This includes two groups of parameters to be optimized, namely (a) dimensional, L^*, T^*, and e_a^* with units $[L]$, $[T]$, and $[e_\mathrm{a}]$, respectively, and (b) dimensionless η_T, η_e, $a_{\mathrm{CO_2}}$and a_C. Excepting the last one, referring to the cloud area fraction, C, and discussed in Section 4.2, all others were optimized based on clear-sky MODTRAN results, and their values are contained in Table 1.

Table 1: Fitted parameters of Equation (2) for ranges of temperature 247.2 to 309.7 K (–26.0 to 36.6 °C), water vapour pressure 1.08 to 20.9 hPa, and CO_2 concentration 200 to 800 ppm.

	Sign†	L^* (W/m²)	T^*(K)	e_a^* (hPa)	$[\mathrm{CO_2}]_0$ (ppm)‡	η_T	η_e	$a_{\mathrm{CO_2}}$	a_C§
Downwelling, L_D	+	27	181	6.36	400	4.5	1	0.015	0.34
Outgoing, L_O	–	1	55	0.00302	400	3.5	0.5	0.015	0.15

† *Specific sign to replace ± in Equation (2).*
§ *These are global values; for values of outgoing radiation per geographical zone see Figure 13.*
‡ *Not necessary to optimize.*

As seen in Table 2, the performance measures of the fitting are very good and hence the equation is a good macroscopic representation of the MODTRAN results. The good performance is also seen graphically in Figure 9 for downwelling flux and Figure 10 for outgoing flux.

Table 2: Performance indices of Equations (2) (with parameters as in Table 1) and (3), fitted for ranges of temperature 247.2 to 309.7 K (–26.0 to 36.6 °C), water vapour pressure 1.08 to 20.9 hPa, CO_2 concentration 200 to 800 ppm, and clear sky.

Equation, variable	Range of L (W/m^2)	RMSE† in L (W/m^2)	NSE§ of L (%)	RMSE† in relative error $(L^e - L)/L$ (%)	Maximum absolute relative error $\lvert L^e - L\rvert/L$ (%)
(2), downwelling, L_D	140.0 – 419.5	1.3	99.97	0.5	1.9
(2), outgoing, L_O	170.6 – 351.1	1.3	99.79	0.7	1.9
(3), outgoing, L_O from L_D	170.6 – 351.1	3.6	99.24	1.5	4.5

† *Root mean square error.*
§ *Nash-Sutcliffe efficiency (defined to be the difference from 1 of the ratio of the mean model square error to the variance of the variable that is modelled).*

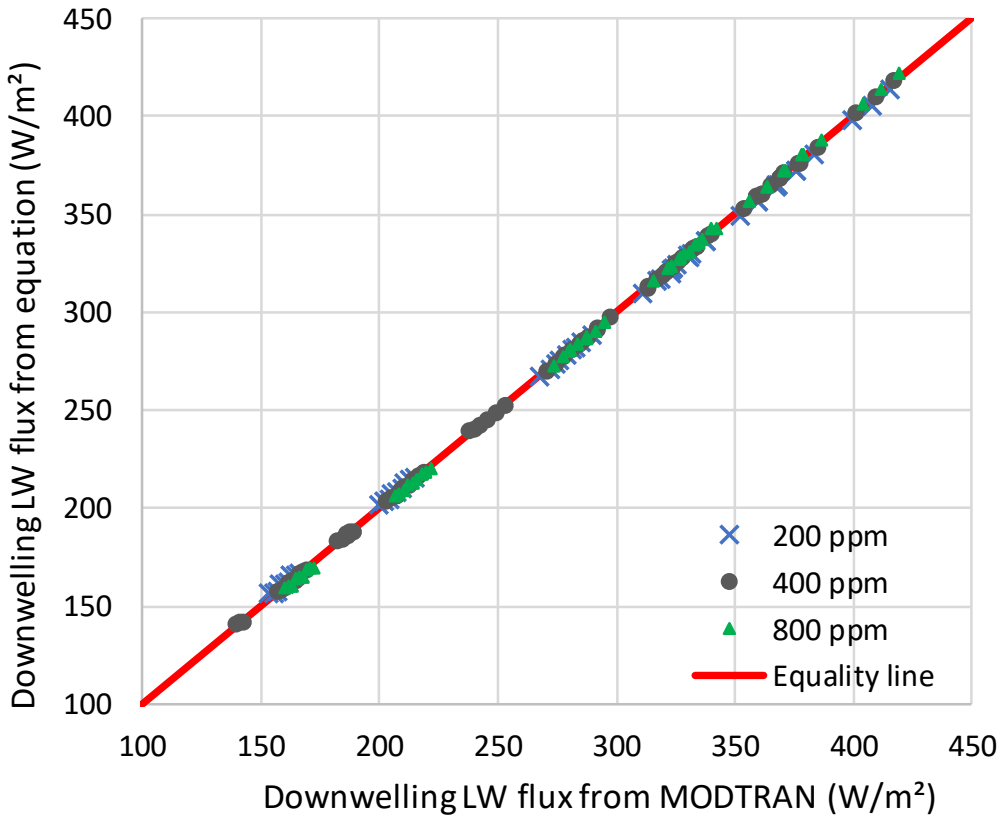

Figure 9: Comparison of downwelling LW radiation flux, L_D, as computed by MODTRAN and by Equation (2).

For completeness, an additional equation was formulated, which directly relates the outgoing to the downwelling radiation. It is very simple:

$$L_O = L_s - \frac{L_D}{2} + 40\ \mathrm{W/m^2} \tag{3}$$

where to calculate the surface radiation flux L_s the emissivity was taken $\varepsilon_s = 0.97$. The performance of Equation (3) is also good, albeit inferior to that of Equation (2), as seen in Table 2 and Figure 11. This equation shows that the outgoing and downwelling fluxes are closely (and negatively) correlated to each other.

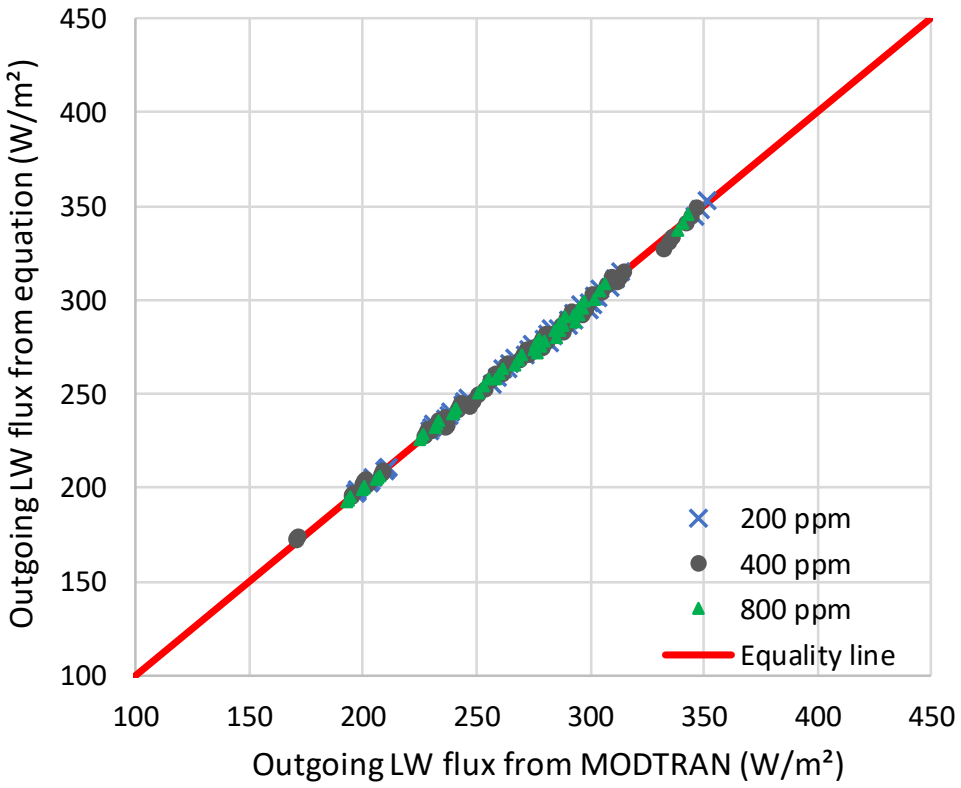

Figure 10: Comparison of outgoing LW radiation flux, L_O, as computed by MODTRAN and by Equation (2).

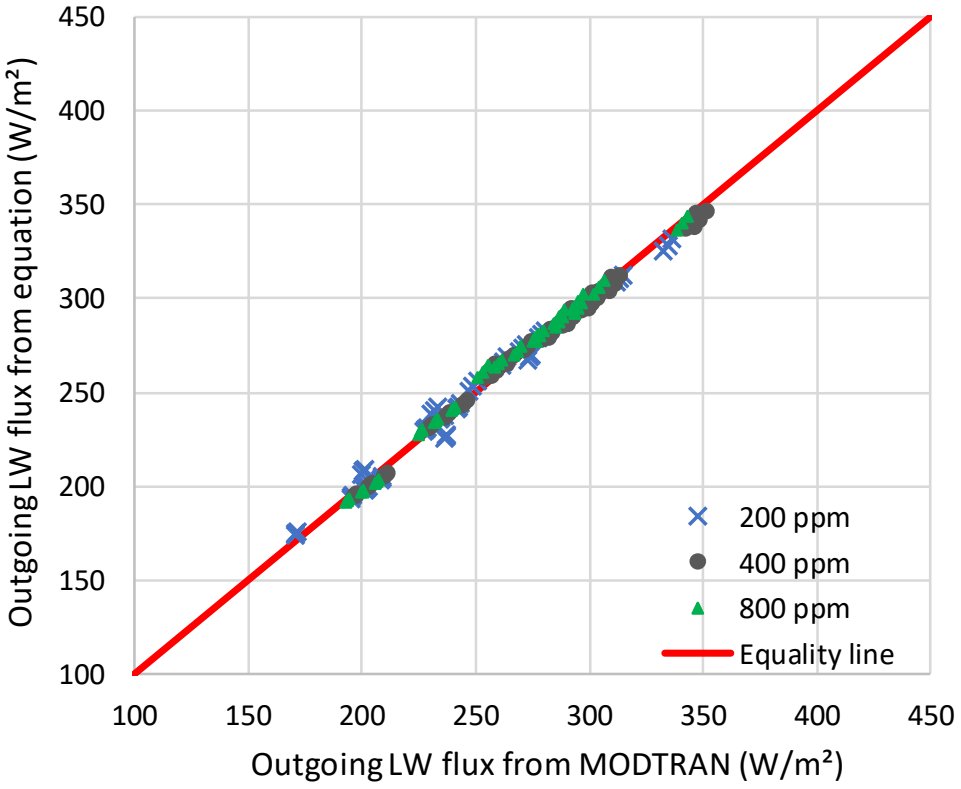

Figure 11: Comparison of outgoing LW radiation flux, L_O, as computed by MODTRAN and by Equation (3), based on the downwelling flux, L_D.

4.2 Effect of Clouds

MODTRAN offers the possibility to model different types of clouds, in addition to clear-sky conditions. Figure 12 shows an example for cumulus clouds and the tropical profile. In particular, it shows that Equation (2) with $(1 - a_C C) = 0.904$ (standing for the ratio of outgoing radiation under cloudy sky to that of clear sky) also represents well the case of cumulus clouds without changing the parameters. Similar performance appears for other types of clouds, but with different ratios, which are shown in Table 3 for the different types of clouds and locality profiles.

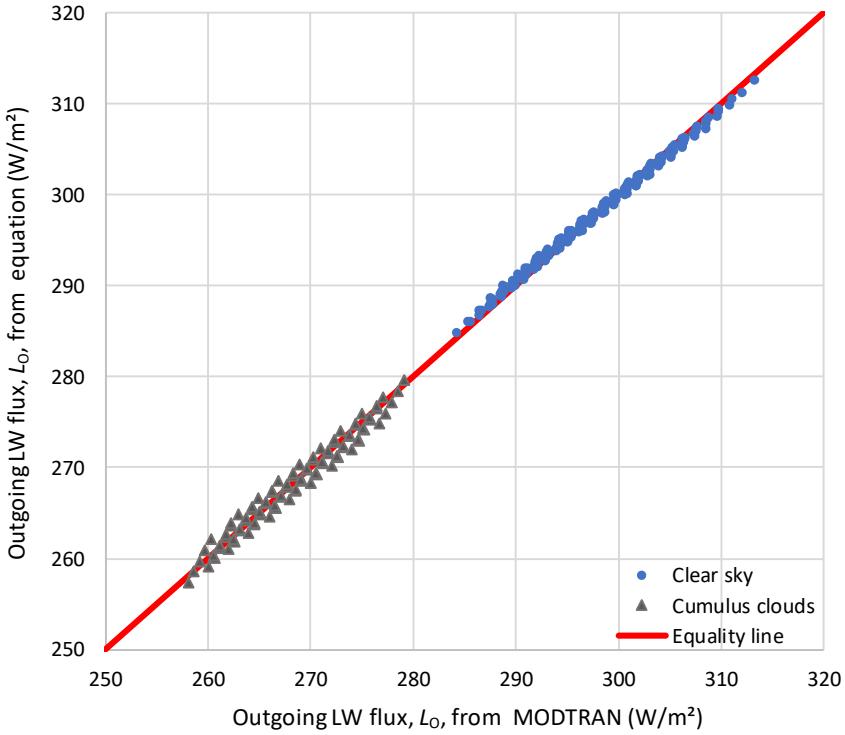

Figure 12: Comparison of outgoing LW radiation flux, L_O, as computed from MODTRAN and from Equation (2), fitted only for the tropical profile and for T = 299.7 ± 2 K, e_a = 19 ± 1.9 hPa, and [CO_2] range of 200 – 800 ppm. The parameters of Equation (2) were reoptimized for these ranges, and the values T^* = 56.2 K and $e_a^* = 0.00683$ hPa were found, while all others remained the same as in Table 1. The case of cumulus clouds is also plotted in the graph, with abscissae as derived by MODTRAN and ordinates equal to the values of Equation (2) for clear sky multiplied by 0.904.

Table 3 *Ratios of outgoing LW radiation under cloudy sky to that for clear sky, for the indicated types of clouds and locality profiles, as determined by MODTRAN for default settings (the lowest value is highlighted in bold).*

Locality profile → Cloud type ↓	Tropical	Midlatitude summer	Subarctic summer	Midlatitude winter	Subarctic winter
Cumulus	0.904	0.899	0.889	0.910	0.95
Altostratus	0.901	0.896	**0.887**	0.907	0.948
Stratus	0.966	0.973	0.962	0.973	1.016
Stratus/Stratocumulus	0.939	0.945	0.931	0.950	0.989
Nimbostratus	0.98	0.984	0.977	0.984	1.024
Standard Cirrus	0.93	0.939	0.957	0.95	0.974
NOAA Cirrus	0.937	0.945	0.963	0.956	0.98

However, it is important to test whether these ratios agree with observed ones. From the CERES data sets, the global average LW radiation flux for the entire observation period, 2001 – 2022, is $L_O^{CS} = 268.2$ W/m² for clear sky and $L_O^{AS} = 239.5$ W/m² for all sky, and give a ratio of 0.892. On

the other hand, the global average cloud area fraction, again calculated from the CERES data, is $C = 0.671$. We assume that the following approximation holds:

$$\frac{L_{\mathrm{O}}^{\mathrm{AS}}}{L_{\mathrm{O}}^{\mathrm{CS}}} = 1 - a_{\mathrm{O}} C \tag{4}$$

from which we find $a_{\mathrm{O}} = (1 - 0.892) / 0.671 = 0.161$. For $C = 1$, we would have $L_{\mathrm{O}}^{\mathrm{AS}} / L_{\mathrm{O}}^{\mathrm{CS}} = 0.839$. Comparing the latter value to those in Table 3, we understand that the MODTRAN model severely underestimates the effect of clouds, as even the least value of the ratio in the Table (0.887 for altostratus clouds and the subarctic summer profile) is too high in view of an average of 0.839. Therefore, to model the effect of clouds we use the CERES data rather than the MODTRAN results, based on the simple relationships:

$$L_{\mathrm{O}}^{C} = L_{\mathrm{O}}(1 - a_C C), \qquad L_{\mathrm{D}}^{C} = L_{\mathrm{D}}(1 + a_C C) \tag{5}$$

where L_{O} and L_{O}^{C} denote the outgoing LW radiation flux for clear sky and cloudiness C, respectively (and likewise for the downwelling, L_{D} and L_{D}^{C}), and a_C is a dimensionless parameter, which may take different values for different situations. These relationships are already incorporated in Equation (2). To determine the parameter a_C for the outgoing LW radiation, we investigate the CERES data (clear and all sky, and cloud fraction, globally and in the five different geographical zones, as shown in Figure 13.

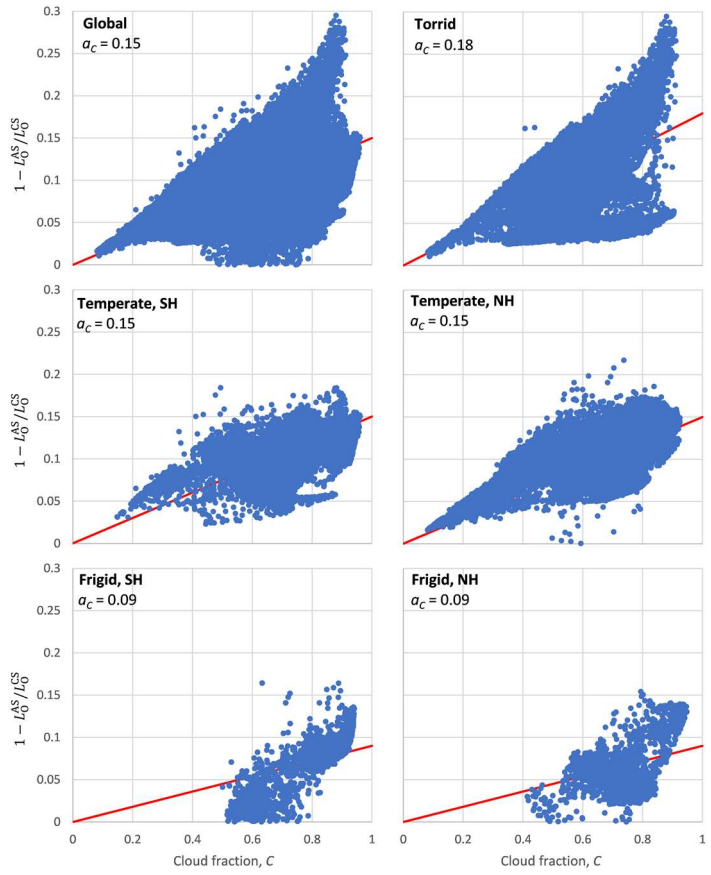

Figure 13: Effect of clouds to outgoing radiation, expressed as $1 - L_O^{AS}/L_O^{CS}$, i.e. the deviation from 1 of the ratio of longwave radiation for all sky (L_O^{AS}) to that for clear sky (L_O^{CS}), vs. the cloud fraction, C. The slopes of homogenous linear regressions, a_C are also shown. Each plotted point corresponds to one of the 64 800 grid points of the CERES grids of clear-sky and all-sky radiation (Figure 2), and cloud area fraction (Figure 3), where the average over the period 2001-2022 was taken.

The resulting a_C values are also shown in Figure 13 and vary from 0.18 in the torrid zone to 0.09 in the frigid zones. Notable is the large spread of the observations, with a variation range of 0 to about twice the estimated mean slope (i.e., $1 - L_O^{AS}/\, L_O^{CS}$ from 0 to 0.30). For a detailed deterministic modelling, this spread would not be acceptable, but in a macroscopic modelling within stochastics, Figure 13 provides useful and utilizable information.

The data used in this study do not allow direct estimation of a_C for downwelling flux and thus we use values from literature. Dingman (1994, p. 189) suggested a value of 0.4, Jacobs (1978, p. 108) estimated a value of 0.33 and Lhomme et al. (2007) a value of 0.34. (This could be also taken as 0.37 as the formula in their equation (13) can be written as is $L_D^C/L_D = 1.03 + 0.34\, C$, which for $C = 1$ yields $L_D^C/L_D = 1 + 0.37$.) Of these values, here we use $a_C = 0.34$ as this value was based on the most extensive data set and is the most recent. Other researchers give different formulae (Brutsaert, 1991, p.142; Carmona et al., 2014; Wong et al., 2023), but here we preferred the simplest linear formulation.

5. Testing of Model Results

5.1 Radiation Flux Profiles

As already mentioned (Section 3), the most appropriate way to test the validity of a model that determines the LW radiation, such as MODTRAN, would be to compare its results to observed radiation profiles. As described in Section 3, here we make a single comparison to get a general idea, using the two radiosondes launched on 23 September 2011 at Payerne, Switzerland, and reported in the study by Philipona et al. (2012), whose LW radiation profiles were digitized here. As reported in the study, the surface-emitted LW upward radiation was about 445 W/m² during the day, with a remarkably strong decrease during the first 1 km, and 380 W/m² during the night. A surface temperature of 11 °C (284.2 K) is reported in the study for 23 September 2011, without clarifying whether this corresponds to the day or night radiosonde. Using MODTRAN with the standard midlatitude summer profile, we find that at the altitude of +0.5 km, the values of 445 W/m² and 380 W/m² are achieved for a temperature offset of +5.5 K (297.5 K at +0.5 km) and −6.2 K (285.8 K at +0.5 km, close to the reported 284.2 K), respectively. However, the former temperature offset gives too high temperature at higher altitudes, inconsistent with the observed strong decrease across the first 1 km. Therefore for the comparison of the day profile with MODTRAN we did not use any temperature offset, while for the night case we assumed an offset of –6.8 K (285.1 K, midway of the values 284.2 K and 285.8 K).

Figure 14 depicts the radiosonde profiles, compared with the MODTRAN results obtained with the above assumptions. For the night radiosonde, there is a good agreement, yet the differences between observations and MODTRAN results are ±25% for the downward flux and ±4% for the upward flux. For the day radiosonde, the differences are substantial, particularly above 7 km. Philipona et al. (2012) attribute these differences to the thermal longwave radiation from the Sun—a plausible interpretation. Excepting the latter factor, we may deem that MODTRAN represents the relevant processes satisfactorily.

5.2 Downwelling Radiation

As already mentioned, we use the empirical or semi-empirical formulae of downwelling radiation to test the MODTRAN results. These formulae are expressed in terms of emissivity $\varepsilon_a = L_D/\sigma T_a^4$ (Appendix A). Figure 15 shows that the emissivity calculated by the macroscopic relationship of Equation (2) perfectly agrees with that directly calculated by MODTRAN, with a Nash-Sutcliffe efficiency NSE = 99.9%. As seen in Figure 16, the agreement is not so good if we compare MODTRAN's emissivity with those of the formulae in Appendix A. The best agreement (NSE = 61.6%) is seen for Prata's Equation (A14) followed by Brutsaert's Equation (A12) (NSE = 39.5%) and the FAO Penman-Montieth's Equation (A19) (NSE = 1%). The Brunt / Penman Equation

(A17) gives a NSE < 0, meaning that a single value equal to the mean performs better than the relationship in representing the compared data.

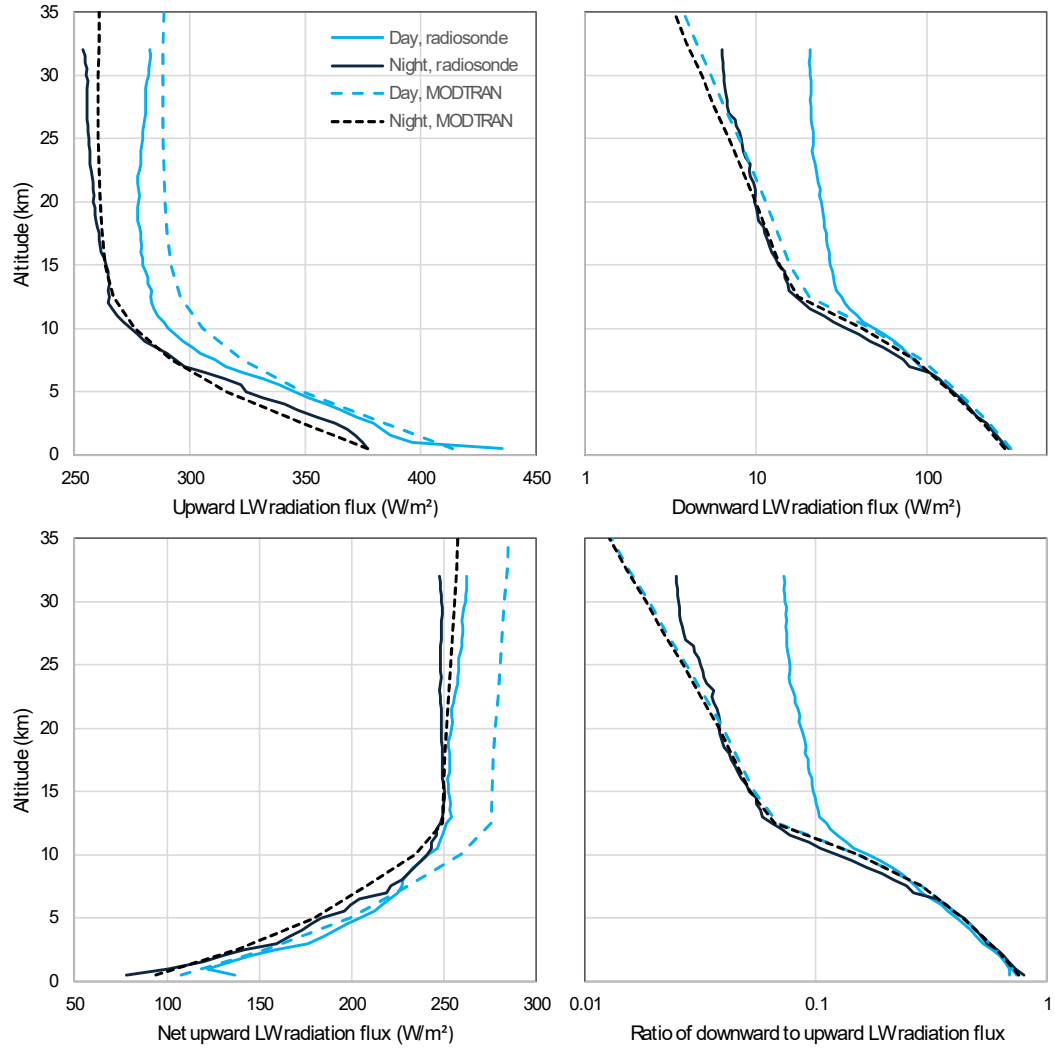

Figure 14: Comparison of LW radiation components calculated by MODTRAN to radiosonde measurements by Philipona et al.(2012).

Note that if the group of points corresponding to subarctic winter with temperatures lower than 270 K is excluded, Brutsaert's equation has the best performance of all, with a NSE of 75%. Overall, if we assume that the empirical or semi-empirical formulae are closer to reality than MODTRAN because they are based on data and if we exclude the subarctic winter data (and the Brunt / Penman equation) we conclude that MODTRAN underestimates the downwelling radiation flux.

Another comparison is made in Figure 17 for the downwelling LW radiation flux vs. temperature, as calculated by MODTRAN and the CERES EBAF zonal distribution shown in Figure 4. For the former, all five locality profiles are used with default settings as well as with temperature offsets from the default values of up to ±25 K. We recall that CERES EBAF data are not actually measurements but computed results. Yet the graph suggests a tendency of MODTRAN to underestimate the downwelling radiation, a finding similar to that in the comparison with the emissivity formulae.

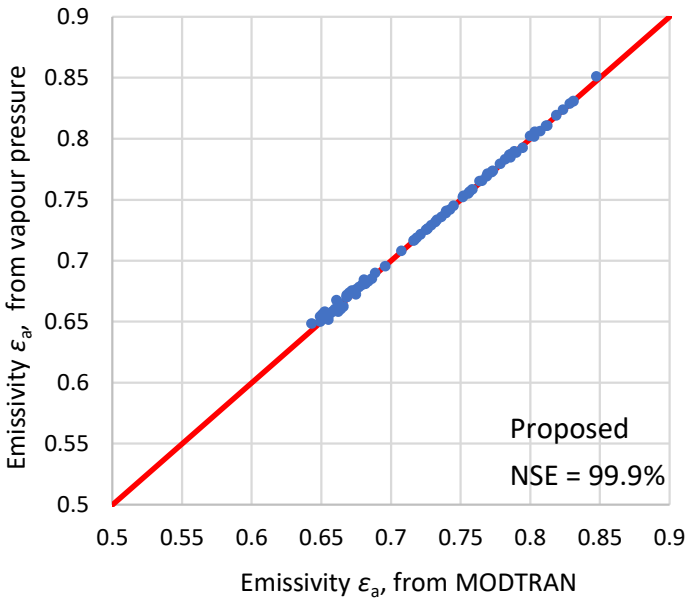

Figure 15: Comparison of emissivity calculated by MODTRAN to that calculated by Equation (2).

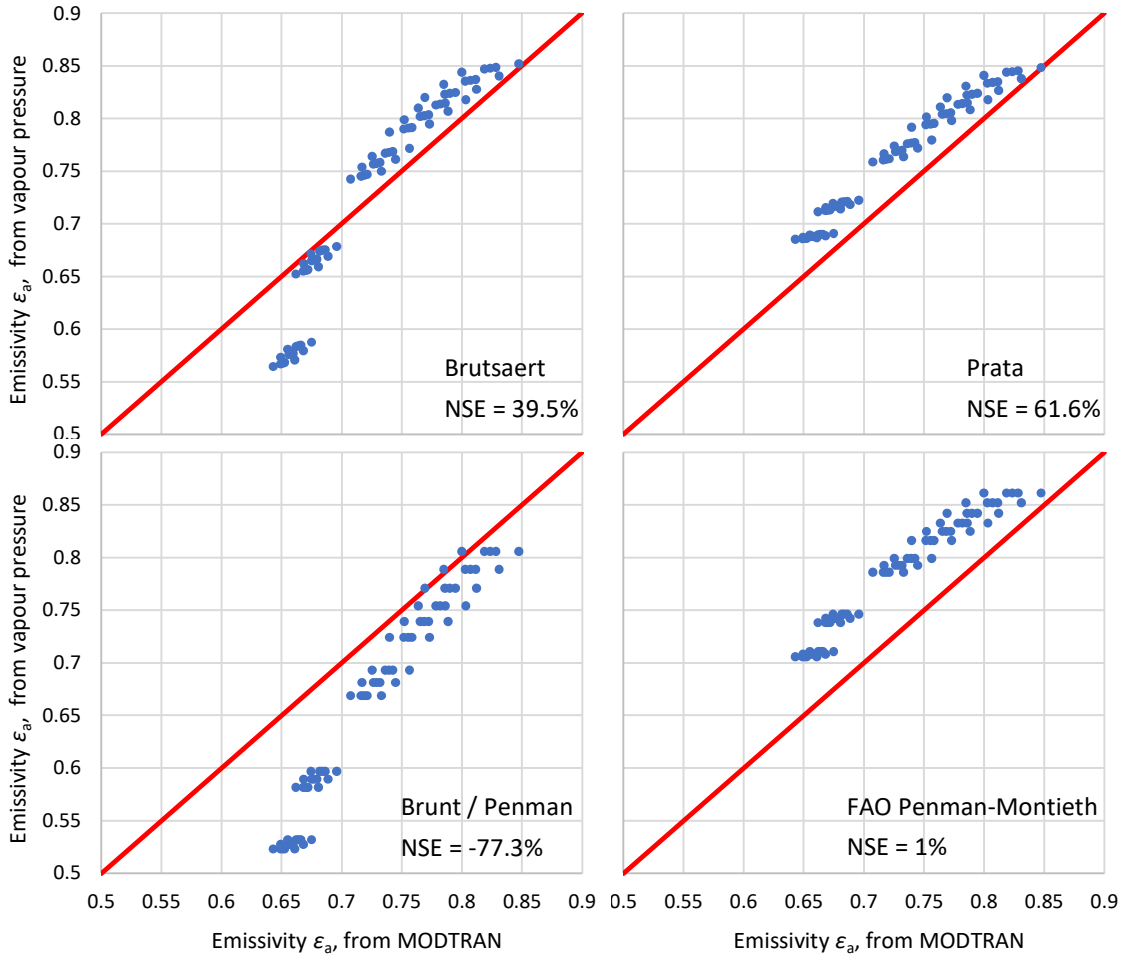

Figure 16: Comparison of emissivity calculated by MODTRAN to that calculated by each of the indicated formulae; the Nash-Sutcliffe efficiency (NSE) is also shown for each case.

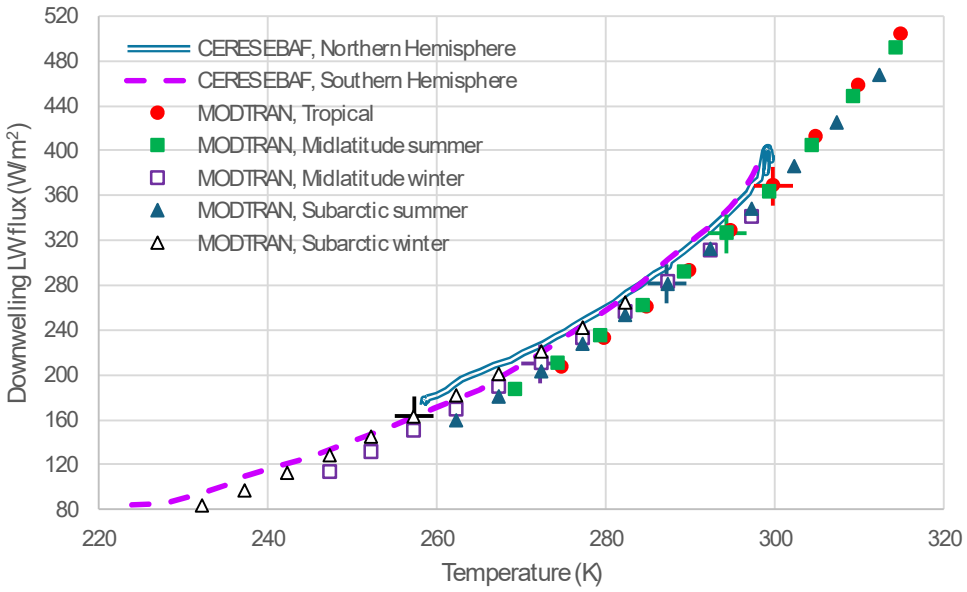

Figure 17: Downwelling LW radiation flux vs. temperature, as calculated by MODTRAN for the five indicated locality profiles and default settings (points with crosses) as well as with temperature offsets from the default values of up to ±25 K (all other points), in comparison to the CERES EBAF zonal distribution shown in Figure 4.

5.3 Outgoing Radiation

For the outgoing radiation, a comparison similar to that in Figure 17 is made. It is presented in Figure 18 and is now stronger and more meaningful, as the CERES outgoing LW flux is observed, rather than a model output. The graph shows that at the default temperature values of each of the MODTRAN profiles, there is almost perfect agreement between CERES data and MODRTAN results, and this is also extended for negative temperature offsets in MODRTAN. However, for positive temperature offsets, MODRTAN overestimates the flux.

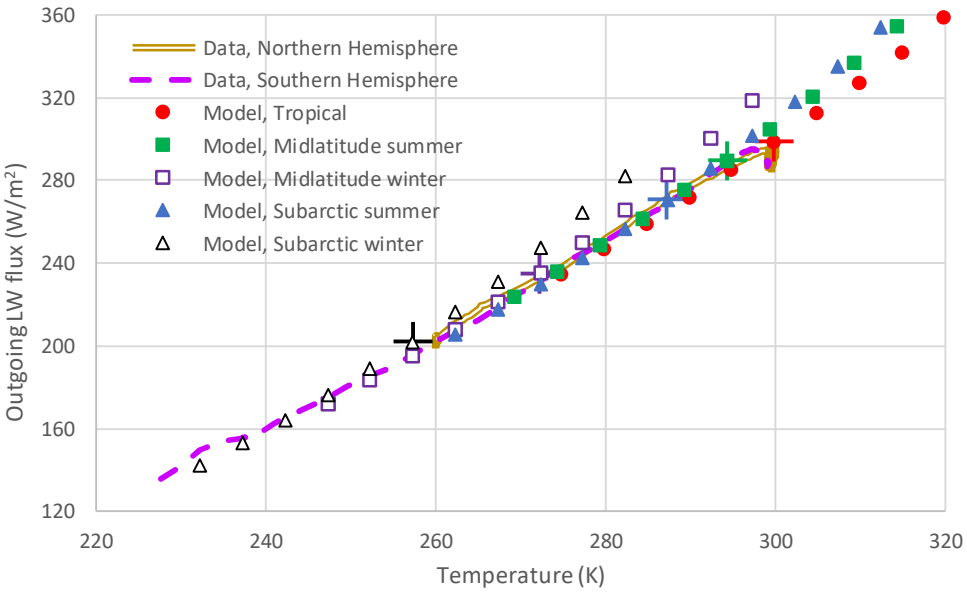

Figure 18: Outgoing LW radiation flux vs. temperature, as calculated by MODTRAN for the five indicated locality profiles and default settings (points with crosses) as well as with temperature departing from the default values by up to ±25 K (all other points), in comparison to the observed zonal distribution (CERES SSF1) as shown in Figure 4 and Figure 6.

As another test, we use time series of meteorological variables and [CO_2] for the 22 years of CERES data availability averaged over the torrid zone, which are shown in Figure 19.

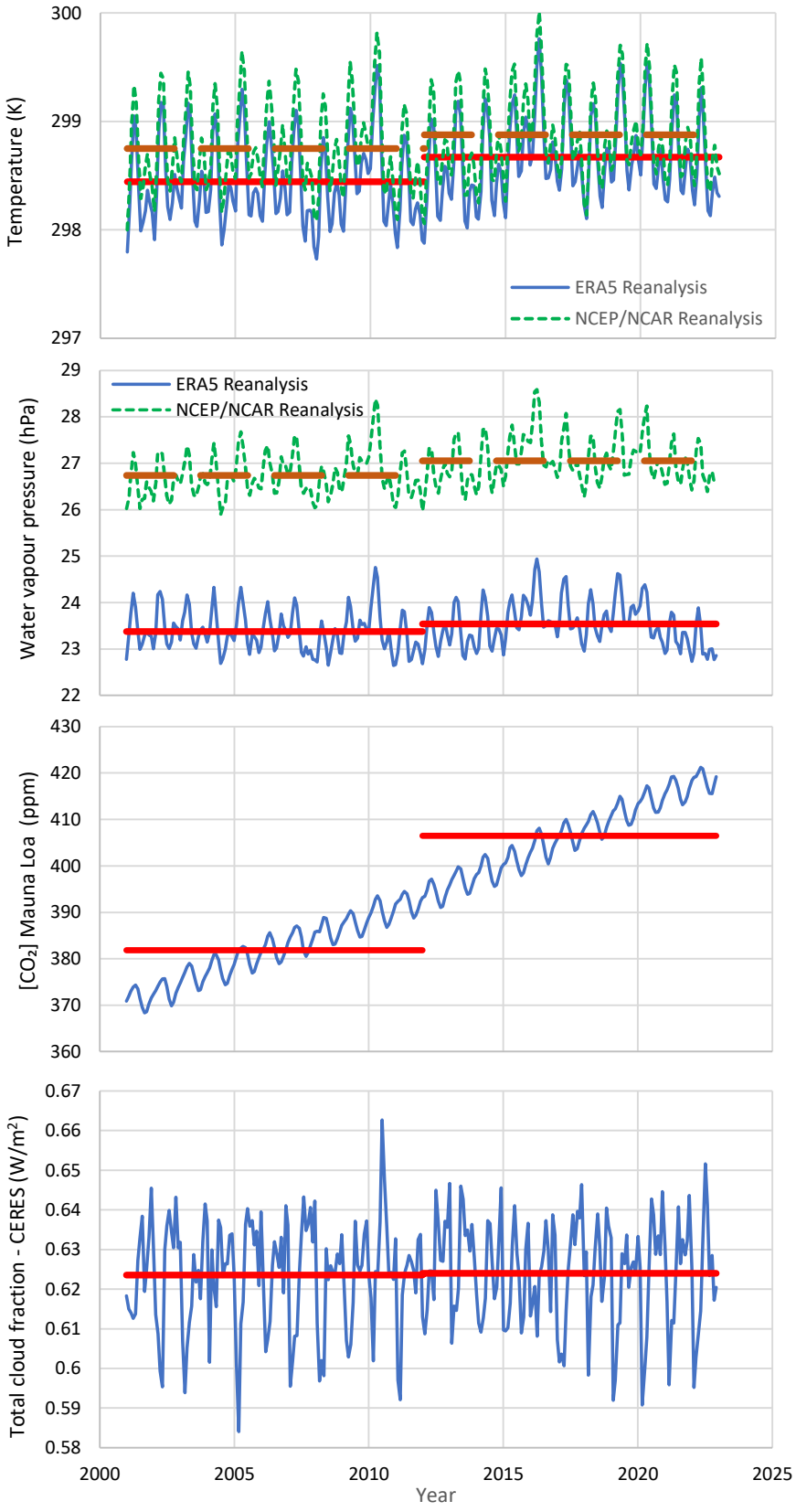

Figure 19: Time series of the indicated variables averaged over the torrid zone. The values plotted are monthly averages, while the 11-year averages are also plotted in thicker (red or dark red) lines.

For temperature and water vapour pressure, both ERA5 and NCEP/NCAR reanalyses data are used, which, as shown in the graphs, have differences from each other, particularly in the latter variable. Based on these time series and Equation (2), the model results, which correspond to MODTRAN, are calculated and plotted in Figure 20. In the upper panel of the Figure, substantial differences are seen in the mean levels of the clear-sky LW outgoing radiation, both between the time series of the two reanalyses and the latter with the CERES data. These can be attributed mostly to uncertainty in reanalyses data and their representation of reality, as indicated in the differences between the two. If we exclude the effect of the mean level differences, the cross-correlation coefficients with the CERES data are reasonable, i.e. 0.67 for ERA5 and 0.69 NCEP/NCAR.

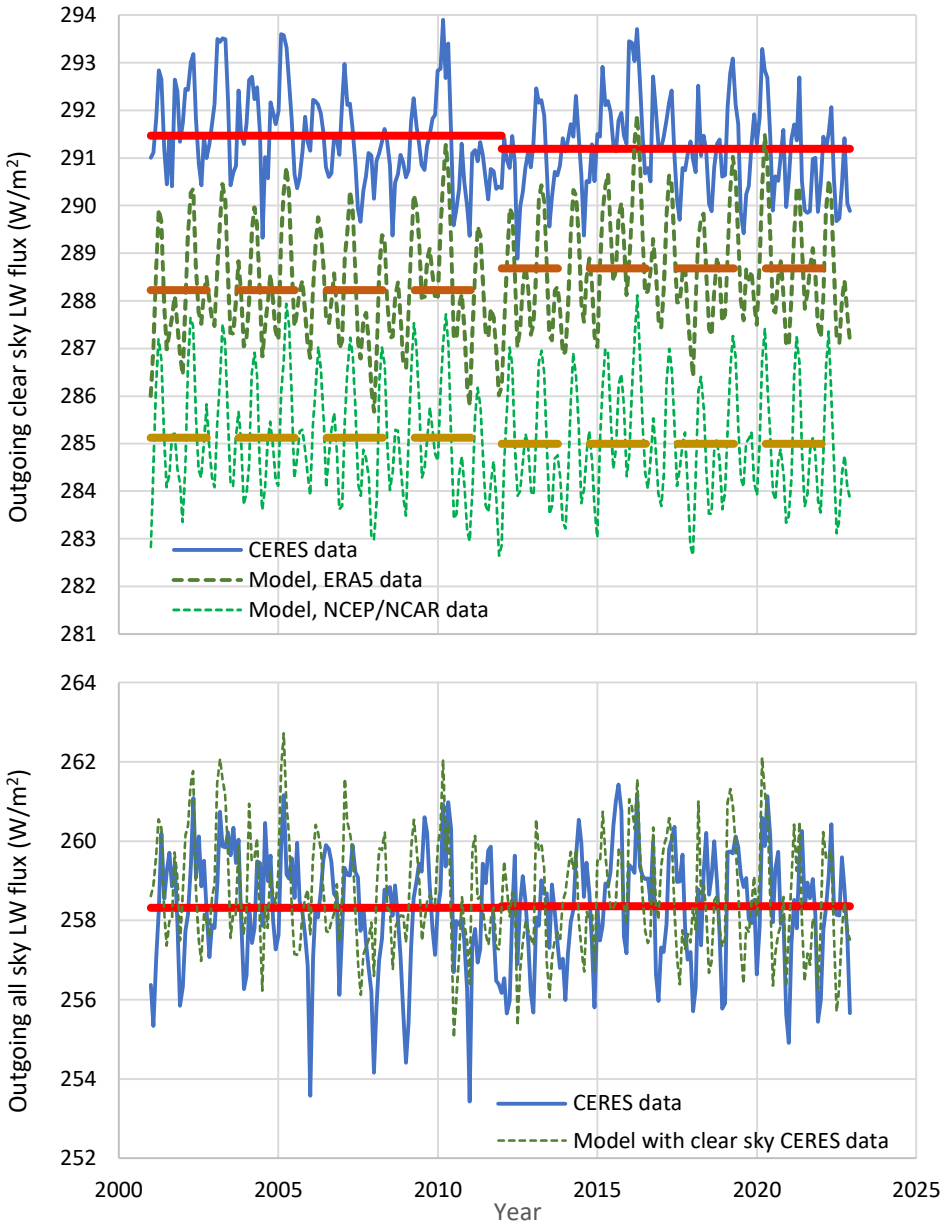

*Figure 20: **(upper)** Time series of outgoing clear-sky LW radiation flux, averaged over the torrid zone, as given by CERES data and as predicted by Equation (2) with temperature, water vapour and [CO_2] data from the ERA5 and NCEP/NCAR Reanalyses. **(lower)** Time series of outgoing all-sky LW radiation flux, averaged over the torrid zone, as given by CERES data and as predicted by the CERES clear-sky data and Equation (2) with CERES cloud area fraction. The values plotted are monthly averages, while the 11-year averages are also plotted in thicker (red or dark red) lines.*

In the lower panel of Figure 20, we use the CERES clear-sky time series, as shown in the upper panel, and multiply it by the quantity $(1 - a_C C)$ of Equation (2), with $a_C = 0.18$ (the value of the torrid zone) and cloudiness C as in the time series of the lowest panel of Figure 19. The attained results compare well with the all-sky CERES time series in terms of mean level, even though the cross-correlation between the two plotted time series (–0.15) does not suggest correspondence of the individual monthly values.

In both Figure 19 and Figure 20, the average values of the time series are shown for two 11-year subperiods, 2001 – 2011 and 2012 – 2022. It is seen that there were increases in the second period in all variables (very large in CO_2 and very slight in all-sky outgoing radiation) except in the clear-sky radiation, where a slight decrease (–0.08 W/m^2) is seen. It is interesting to investigate if the latter decrease is explained by MODTRAN. The results of the related calculations are shown in Table 4. Using any of its default profiles, MODTRAN results in an increase of outgoing clear-sky LW radiation (from +0.38 to +0.60 W/m^2), opposite to what is seen in the CERES data.

Table 4 *Comparison of observed data and MODTRAN results for the average conditions of each of the indicated two periods. The observed data are global averages. The MODTRAN results are for the average observed temperature and [CO_2] of each period, and for the same water vapour scales in the two periods, estimated so as to (approximately) match the outgoing clear-sky LW flux of CERES for the first period, while holding fixed relative humidity for the two periods.*

Period →	2001-11	2012-22	Difference
Observations (averages over each period)			
Temperature from ERA5 (K)	287.21	287.49	+0.28
[CO_2] from Mauna Loa (ppm)	381.83	406.48	+24.65
Outgoing TOA (20 km) clear-sky LW from CERES (W/m^2)	268.33	268.27	–0.08
Outgoing clear-sky LW radiation by MODTRAN at 20 km altitude (W/m^2)			
Tropical profile, water vapour scale 0.82	268.34	268.72	+0.38
Midlatitude summer profile, water vapour scale 1.08	268.34	268.78	+0.44
Midlatitude winter profile, water vapour scale 1.14	268.28	268.78	+0.50
Subarctic summer profile, water vapour scale 2.56	268.31	268.91	+0.60

The above results from CERES data, which are for the torrid zone only, are similar to those for global averages, presented by Koutsoyiannis and Vournas (2024; Appendix B). The latter study also examined SW radiation data and found a decrease in total outgoing radiation, which is consistent with the increased atmospheric temperature. This decrease in outgoing radiation can hardly be attributed to increased [CO_2] but it can be related to water vapour and cloud profiles. The effect of CO_2 is trumped by the effect of clouds, which is consistent with the major role of water on climate and the minor one of CO_2.

5.4 Final Assessment

The above tests illustrate the high uncertainties not only in the CERES LW radiation data, but also in the other atmospheric variables, and the relationships among them and the LW radiation, as represented in MODTRAN. The uncertainties do not allow accurate representation of quantities calculated as differences between different variables or between the same variables in different periods, which would be required for attribution of changes. On the other hand, the macroscopic behaviour of MODTRAN seems consistent with what is observed for clear sky, and therefore MODTRAN is suitable for the scope of this paper, which is the investigation of the relative importance of carbon dioxide and water in the greenhouse effect, as detailed in the next section. As regards clouds, MODTRAN seems to underestimate their effect, but by using the cumulus or altostratus cloud conditions, we get results close to reality for average all-sky conditions.

6. Comparison of H_2O and CO_2

6.1 Imaginary-world Conditions

Investigating imaginary-world conditions seems pointless, yet we include it for the reasons explained in the Introduction—the fact that several popular narratives are based on imaginary-world conditions. The imaginary-world conditions we examine are the most extreme ones, starting from the case that [CO_2] is totally absent in the atmosphere and ending in the case where the atmosphere is made up entirely of CO_2. Extreme ranges are also examined for other greenhouse gases, including water vapour.

Figure 21 compares detailed MODTRAN outputs for the default case of the tropical profile, with [CO_2] = 400 ppm (and T = 299.7 K, L_0 = 298.49 W/m², water vapour scale = 1; red curves), compared to two cases in which CO_2 is totally absent (blue curves). In the left panel, the water vapour is kept at the same level as in the default case. In order for the outgoing radiation to retain its default value (L_0 = 298.49 W/m²), the temperature must be lowered by 15 K (T = 284.7 K). Notably, by also zeroing water vapour, to match the total outgoing LW flux of the red curve (L_0 = 298.49 W/m²), the temperature should be lowered by 28.5 K (T = 271.2 K, a case not shown in the figure but easily imagined in the middle between the smooth curves of 260 and 280 K). The right panel shows that the temperature can remain at its default value (T = 299.7 K) if the water vapour scale is increased to 1.3, accompanied by cumulus clouds. Note that the 30% increase in the water vapour scale does not violate thermodynamic laws, as the vapour pressure remains below the thermodynamic limit. Therefore, assertions that the terrestrial greenhouse effect would collapse without CO_2 (see Introduction) are false.

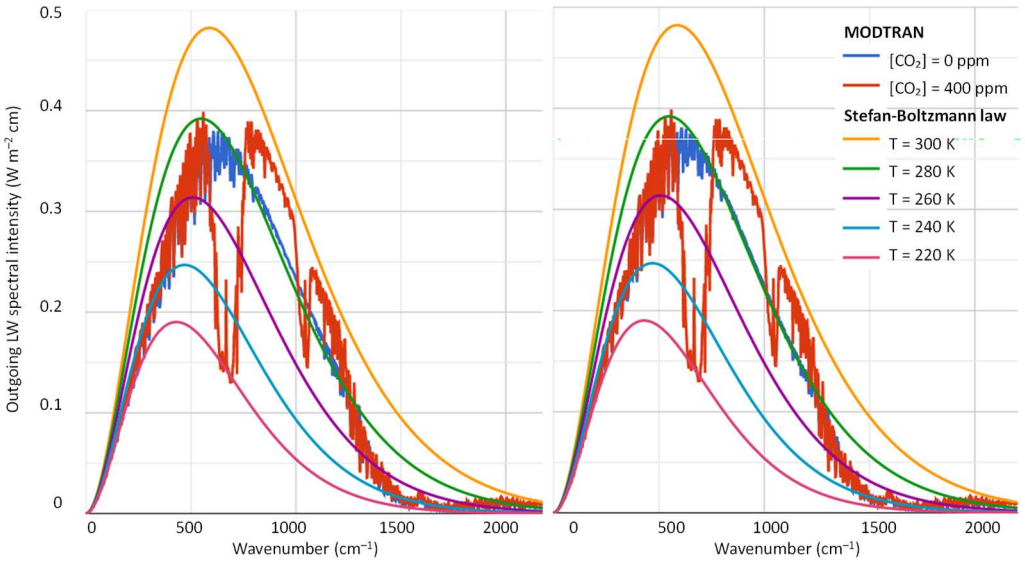

*Figure 21: Output of the MODTRAN model, with the red curves in both panels produced for default settings (for the standard tropical atmospheric profile; T = 299.7 K; [CO_2] = 400 ppm; L_0 = 298.49 W/m²), and the blue curves produced for zero concentrations of all greenhouse gases except water vapour, assuming constant relative humidity and conditions such as to match the total outgoing LW flux of the red curves, namely: **(left)** temperature lower than default by 15 K (T = 284.7 K); **(right)** temperature equal to the default (T = 299.7 K) but water vapour scale increased to 1.3, accompanied by cumulus clouds.*

The fact that the greenhouse effect would not collapse without CO_2 is also shown in Figure 22 (left panel), which gives a more macroscopic picture for both downwelling and outgoing LW flux, under constant temperature equal to that of the standard tropical atmospheric profile (T = 299.7 K) and zero concentrations of all greenhouse gases except water vapour. It is seen that even without any change in the water vapour profile, the difference of LW radiation flux from the value at

the default settings of [CO_2] = 400 ppm is only –3%. With a 10% increase of the water vapour and zero [CO_2], the downwelling radiation matches that for [CO_2] = 400 ppm.

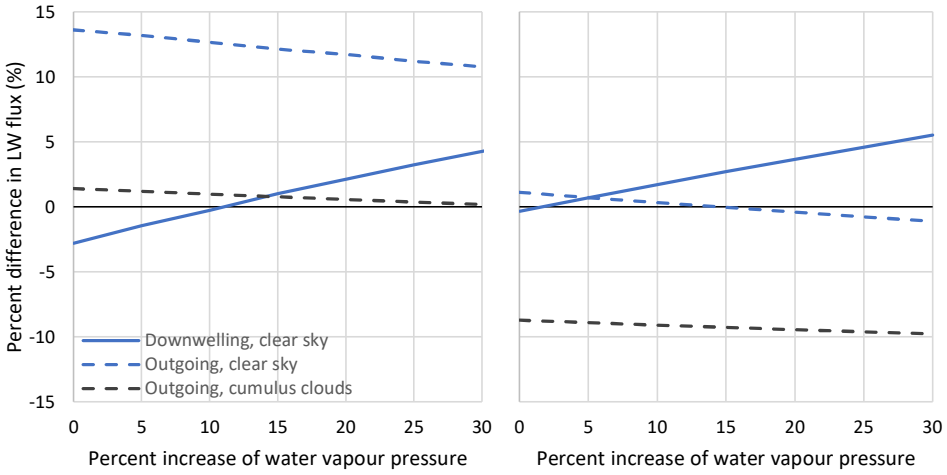

*Figure 22: Difference of LW radiation flux from the values at the default settings of the standard tropical atmospheric profile (T = 299.7 K; [CO_2] = 400 ppm; L_D = 369.26 W/m²; L_O = 298.49 W/m²), as calculated by MODTRAN for the cases of (**left**) zero concentrations of all greenhouse gases except water vapour, assuming constant relative humidity and (**right**) as in left but with [CO_2] = 200 ppm.*

Additional imaginary-world conditions are shown in Table 5. It can be seen there that by removing the entire quantity of atmospheric CO_2 we can achieve the same level of greenhouse effect, as produced by [CO_2] = 400 ppm and zero water vapour, with only 0.15% of the current H_2O level in terms of upward and downward LW heat flux at the surface, or 4% in terms of the outgoing LW heat flux at 100 km altitude. On the contrary, it is impossible to approach the values of the greenhouse effect achieved by H_2O alone in the atmosphere at the current level, by removing it and replacing it with CO_2. Even in an atmosphere entirely composed of CO_2 (i.e. 1 000 000 ppm or 2500 times the current CO_2 concentration), we cannot approach the greenhouse values achieved by the current level of atmospheric H_2O alone. On the other hand, we can easily achieve the greenhouse effect level of an atmosphere entirely composed of CO_2 with an atmosphere free of CO_2 and with only 20% of the current atmospheric H_2O for the downwelling radiation.

Table 5: Results of MODTRAN calculations for tropical profile and temperature at zero altitude of either 288 K (the value of current global temperature used by Brutsaert, 1975) or 299.7 K (the standard value of temperature at zero altitude of the tropical profile) and for extreme (imaginary-world) cases of greenhouse gas concentrations.

[CO_2] relative to the default value of 400 ppm	Water vapour scale relative to the default tropical profile	Other greenhouse gases concentration relative to default	Downward LW heat flux at surface (W/m²)	Upward LW heat flux at surface (W/m²)	Outgoing LW radiation flux at 100 km altitude (W/m²)
1	1	1	325.6 (369.3)*	381.5 (446.5)	249.5 (298.5)
1	1	0	324.0 (366.8)	381.5 (446.5)	256.7 (307.1)
0	0	0	1.7 (2.2)	380.3 (445.3)	379.0 (443.7)
1	0	0	68.2 (80.9)	380.3 (445.3)	340.7 (400.4)
2500†	0	0	215.7 (259.0)	381.5 (446.8)	257.1 (302.2)
0	0.0015	0	78.8 (90.0)	380.3 (445.3)	366.4 (449.6)
0	0.04	0	157.8 (183.3)	380.6 (445.6)	340.7 (399.7)
0	0.2 (0.27)*	0	212.5 (259.7)	380.9 (445.9)	319.3 (370.2)
0	1	0	319.7 (358.9)	381.5 (446.5)	284.7 (339.1)
0	2.2 (2.6)	0	372.1 (438.3)	381.8 (447.1)	257.7 (302.6)

* The values without and with parentheses correspond to a temperature at zero altitude of 288 K and 299.7 K, respectively. When there is no parenthesis in the column of water vapour scale, the same scale is assumed for both cases.
† In this case the atmosphere is entirely composed of CO_2 (2500 × 400 = 1 000 000 ppm = 1).

For completeness, we note that MODTRAN does not modify the temperature profile in the case that water vapour is removed. It assumes a temperature gradient of 6.5 K/km, as in the standard atmosphere, or lower. However, without water vapour, the temperature gradient would be the dry adiabatic one, i.e. 9.8 K/km (see Figure 25 discussed in Section 7), which signifies another effect of water vapour on the atmospheric processes. And of course, without water vapour, clouds would not exist and the surface cooling effect would be larger.

6.2 Realistic Conditions

Leaving aside the imaginary-world cases of an atmosphere without CO_2 or one made up entirely of CO_2, we may assume a realistic minimum value of $[CO_2]$ of the order of 200 ppm. Redrawing the left panel of Figure 22 under this minimal value, instead of zero, we get what appears in the right panel. It is obvious that, in comparison to the $[CO_2]$ level of 400 ppm, the differences are small and can be easily counterbalanced by slight changes in water vapour pressure.

Another view of the same is provided by Figure 23, where the differences from the $[CO_2]$ level of 400 ppm for two cases, doubling or halving this level, are presented. While in Figure 22 at zero altitude the temperature is fixed at $T = 299.7$ K and the water vapour pressure is varying, in Figure 23 the water pressure is fixed at its default value (19 hPa) and the temperature is varying (by offsetting the default value) over a wide range, 50 K. The differences are of the order of 1% and do not reach 2%.

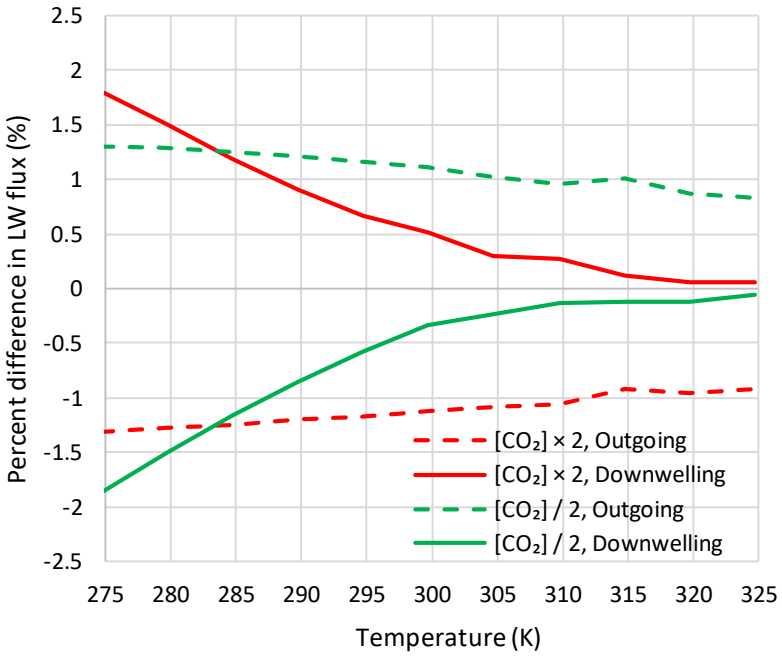

Figure 23: Difference of LW radiation flux for the indicated conditions of $[CO_2]$ from the respective values at the default settings of the standard tropical atmospheric profile (T = 299.7 K; $[CO_2]$ = 400 ppm; L_D = 369.26 W/m²; L_O = 298.49 W/m²), as calculated by MODTRAN.

While the above graphs are suggestive of the low importance of $[CO_2]$ in realistic real-world conditions, here we propose a more advanced method to quantify its relative importance in a more general and systematic manner. Let L be a quantity of interest—in our case the LW radiation flux—that depends on several factors F_i, the explanatory variables. To determine the relative importance of each of the factors F_i, we consider the relative change $\delta L/L$ produced by a relative change $\delta F_i/F_i$ in the factor F_i and we take the ratio:

$$\frac{\delta L}{L} \Big/ \frac{\delta F_i}{F_i} = \frac{\delta L}{\delta F_i} \frac{F_i}{L} \tag{6}$$

As δF_i becomes small, the ratio $\delta L/\delta F_i$ tends to the partial derivative $\partial L/\partial F_i$ and hence the above quantity becomes

$$\frac{\partial L}{\partial F_i} \frac{F_i}{L} = \frac{L'_{F_i} F_i}{L} =: L^{\#}_{F_i} \tag{7}$$

where $L'_{F_i} := \partial L/\partial F_i$ is the partial derivative of L with respect to F_i and $L^{\#}_{F_i} := \partial \ln L/\partial \ln F_i$ is the partial log-log derivative (LLD) of L with respect to F_i. Details about the properties of the LLD are given in Koutsoyiannis (2023, p. 97).

Considering all explanatory variables, the total differential is

$$\mathrm{d}L = \sum_i \frac{\partial L}{\partial F_i} \mathrm{d}F_i \tag{8}$$

and hence

$$\mathrm{d}(\ln L) = \frac{\mathrm{d}L}{L} = \sum_i \frac{\partial L}{\partial F_i} \frac{F_i}{L} \frac{\mathrm{d}F_i}{F_i} = \sum_i L^{\#}_{F_i} \frac{\mathrm{d}F_i}{F_i} = \sum_i L^{\#}_{F_i} \mathrm{d} \ln F_i \tag{9}$$

The partial LLDs, $L^{\#}_{F_i}$, reflect the relative importance of each F_i. For illustration, let us consider a quantity L affected by two factors F_1 and F_2. A small relative change $\delta F_1/F_1$ in F_1, equal to a, without any change in F_2, will result in a change of the dependent quantity L equal to $(\delta L/L)_1 = L^{\#}_{F_1} \delta F_1/F_1 = L^{\#}_{F_1} a$. Likewise, a small relative change $\delta F_2/F_2$, in F_2, again equal to a, without any change in F_1 will result in a change of $(\delta L/L)_2 = L^{\#}_{F_2} a$. Hence,

$$\frac{(\delta L/L)_1}{(\delta L/L)_2} = \frac{L^{\#}_{F_1}}{L^{\#}_{F_2}} \tag{10}$$

which means that the relative change in the quantity of interest due to changes in the explanatory variable is proportional to the partial LLD. Hence, Equation (9) allows the decomposition of the relative change $\mathrm{d}L/L$ due to the relative change $\mathrm{d}F_i/F_i$ of each of the different explanatory variables. Apparently, if the system studied is nonlinear (as most natural systems are), the partial LLDs are not constant. In this case, we must first specify a point of interest (with its coordinates F_i) and then calculate the partial LLDs for this point. The method is quite general and can be applied to any point of interest.

Now, Equation (2) allows analytical determination of the log-log derivatives and hence the relative importance of each of the factors $F_i \in \{T, e_\mathrm{a}, [\mathrm{CO_2}], C\}$. This is made in Table 6. MODTRAN also includes other greenhouse drivers with minor importance, i.e. CH_4, tropospheric ozone, stratospheric ozone, and freon, which were not modelled in the above analyses. To calculate their bulk contribution, we increased each of the default values in MODTRAN by 5% ($\delta \mathrm{AO}/\mathrm{AO} = 0.05$, where AO stands for "all other"), calculated $\delta L/L$ by MODTRAN for the tropical and subarctic summer profile (for comparisons), and applied Equation (6) to calculate $L^{\#}_{\mathrm{AO}}$, which resulted in values also included in Table 6; the relatively high value in the outgoing flux is primarily due to the influence of the stratospheric ozone.

It can be readily found using the values in Table 6, that the relative importance of water vapour over [CO_2] is 0.207/0.015 = 13.8 times for the downwelling flux, and $(-0.136)/(-0.015) = 9.1$ times for the outgoing flux. The relative importance of clouds over [CO_2] is 0.186/0.015 = 12.4 times for the downwelling flux and (–0.112)/(–0.015) = 7.5 times for the outgoing flux. In other words, each of the related factors, water vapour and clouds, is an order of magnitude more

important than [CO₂] in terms of the greenhouse effect.

Considering all above factors, Equation (9) is written as

$$\mathrm{d}(\ln L) = L_T^{\#}\mathrm{d}(\ln T) + L_{e_\mathrm{a}}^{\#}\mathrm{d}(\ln e_\mathrm{a}) + L_{[\mathrm{CO_2}]}^{\#}\mathrm{d}(\ln[\mathrm{CO_2}]) + L_C^{\#}\mathrm{d}(\ln C) \tag{11}$$

The first term in the righthand side, $L_T^{\#}$, is by far the most important factor determining the LW flux. The other terms describe the greenhouse effect. Excluding the first term, i.e., setting $\mathrm{d}T = \mathrm{d}(\ln T) = 0$, Equation (11) allows breakdown of the relative importance of the different greenhouse drivers. This is presented in Figure 24, where the compound importance of water vapour and clouds is 95% and 87% for the downwelling and outgoing radiation, respectively, while that of [CO₂] is 4% and 5%, respectively.

Table 6: Relative changes of LW radiation fluxes at standard conditions, equal to the global averages, T = 288.6 K, e_a = 15.2 hPa, $[CO_2]$ = 400 ppm, C = 0.671, as calculated analytically and numerically by Equation (2).

Case of relative change	Relative change expression	Numerical value of relative change	
		Downwelling flux	Outgoing flux
$L_T^{\#}$	$\dfrac{\eta_T \left(\frac{T}{T^*}\right)^{\eta_T}}{1 + \left(\frac{T}{T^*}\right)^{\eta_T} \pm \left(\frac{e_\mathrm{a}}{e_\mathrm{a}^*}\right)^{\eta_e}}$	3.18	4.44
$L_{e_\mathrm{a}}^{\#}$	$\dfrac{\pm\eta_e \left(\frac{e_\mathrm{a}}{e_\mathrm{a}^*}\right)^{\eta_e}}{1 + \left(\frac{T}{T^*}\right)^{\eta_T} \pm \left(\frac{e_\mathrm{a}}{e_\mathrm{a}^*}\right)^{\eta_e}}$	0.207	–0.136
$L_{[\mathrm{CO_2}]}^{\#}$	$\dfrac{\pm a_{\mathrm{CO_2}}}{1 \pm a_{\mathrm{CO_2}} \ln \frac{[\mathrm{CO_2}]}{[\mathrm{CO_2}]_0}}$	0.015	–0.015
$L_C^{\#}$	$\dfrac{\pm a_C C}{1 \pm a_C C}$	0.186	–0.112
$L_{\mathrm{AO}}^{\#}$	(see text)	0.006	–0.023

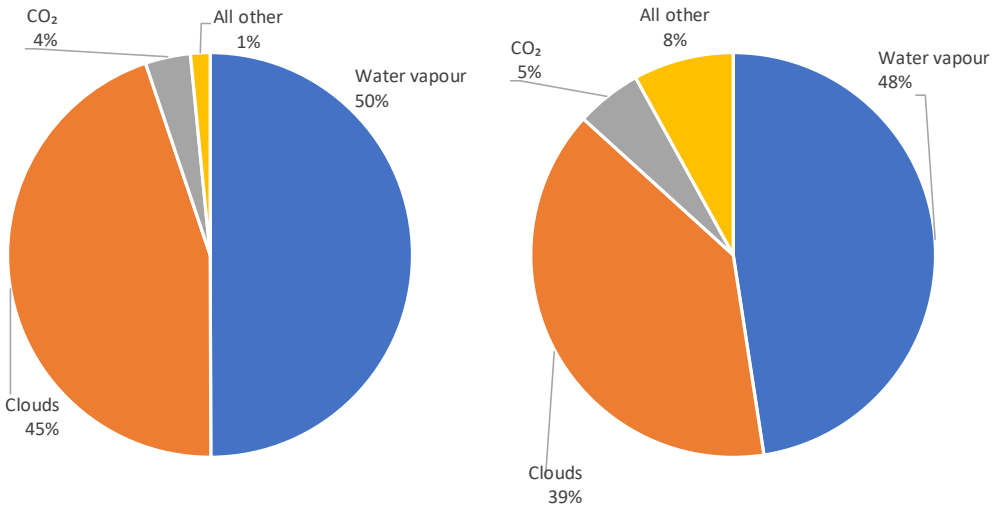

*Figure 24: Contribution of the greenhouse drivers to the LW radiation fluxes, **(left)** downwelling and **(right)** outgoing.*

As Equation (11) is a direct quantification of the greenhouse effect, it provides a means to make simple calculations, which help develop our intuition without resorting to untransparent climate

models. To illustrate this, we consider the example of a relative change in $[CO_2]$ equal to $a = \delta[CO_2]/[CO_2] = \delta \ln[CO_2]$, while the total outgoing LW radiation is constant (i.e. there is no change in the solar constant and the SW radiation process). If there is no change in water vapour and clouds, then this change will be counterbalanced by a temperature increase. Equation (11) with constants as in Table 6, will give $0 = 4.44\,\delta(\ln T) + 0 - 0.015\alpha + 0$ or $\delta(\ln T) = (0.015/4.44)a \approx a/300$. That is, a change of 30% in $[CO_2]$ will result in 0.1% change in T—roughly 0.3 K. If the change in $[CO_2]$ is counterbalanced by a change in water vapour without a change in temperature and clouds, then Equation (11) will give $0 = 0 - 0.136\,\delta(\ln e_a) - 0.015\alpha + 0$ or $\delta(\ln e_a) = -(0.015/0.136)a \approx -a/9$. That is, a change of 30% in $[CO_2]$ can be counterbalanced by a change of about –3% in water vapour pressure. Such calculations do not take into account the interdependence of the different variables, yet they are useful to discern the relative importance in changes thereof.

The above results differ substantially from those of Lacis et al. (2010) and Schmidt et al. (2010), who, using a different methodology, attributed 75% to water vapour and clouds and 19% to CO_2. Our results are closer to an example given by Brooks (1952), in which the contribution of the CO_2 bands is about 1:8 compared to water vapour, without considering the clouds. They are even closer to the results of Harde (2014), who presented exhaustive (line-by-line) spectroscopic calculations based on the detailed representation for high-resolution transmission molecular absorption database HITRAN (2008; a compilation of spectroscopic parameters that a variety of computer codes use to predict and simulate the transmission and emission of light in the atmosphere) and confirmed the domination of water and clouds in the absorption of both the SW and LW radiation. Specifically, Harde found that only about 4% and 3.5% of the total of SW and LW radiation absorption, respectively, can be allocated to carbon dioxide, taking into account the overlap of its spectrum with that of the water vapour (and other greenhouse gases).

For completeness it must be noted that clouds also affect the planet's albedo and the incoming solar radiation, reducing it, but such an analysis is outside the scope of this paper, which is focused on the greenhouse effect. In addition, as already noted, the explanatory variables are not independent from each other. For example, absence of water vapour entails absence of clouds. Additionally, according to the mainstream narrative, an increase of $[CO_2]$ results in increase of water vapour (with the mainstream regarding it to be a feedback of CO_2). But these dependencies, whether true (water vapour – clouds) or not (CO_2 – water vapour, regarded as a feedback) do not invalidate the methodology. The results in Table 6 have been produced for average conditions prevailing in the present atmosphere. If these conditions change because of the dependencies or any other reasons, the partial LLDs should be evaluated at a new point of the vector of explanatory variables.

In this respect, it is useful to estimate the changes that the increase of $[CO_2]$ in a century, from 300 to 420 ppm, may have caused. The results produced by Equation (2), as well as those by direct run of MODTRAN, for this specific increase are shown in Table 7. The former are deemed more reliable than the latter as they are based on a generalized equation representing all conditions, while the latter is based on a specific locality profile, namely midlatitude summer profile (and altostratus clouds for the cloudy case). The change in the downwelling radiation is estimated at 0.5% or lower, which could not be discerned by observations, thus confirming the finding by Koutsoyiannis and Vournas (2024). The change in the outgoing radiation is estimated also at 0.5% (but with a negative sign) or lower (compare also with Salby, 2012, p. 249), which also could not be discerned by observations. Table 7 also shows the expected results for the case that $[CO_2]$ increases to 800 ppm. Now the change in the LW radiation flux is higher, 1.5%, and again could hardly be detected macroscopically by measurements in the future, in case that indeed $[CO_2]$ reaches 800 ppm.

Our results in Table 7 are comparable to those of van Wijngaarden and Happer (2020) (corroborated in de Lange et al., 2022), who, using the HITRAN database and satellite data, concluded that a doubling of CO_2 concentration (from 400 to 800 ppm) would result in a 3 W/m^2 decrease of radiation flux in the top of the atmosphere, which translates to –1.1%. The results in Table 7

are also comparable with those by Harde (2017; tables 2, 4, 5) even though the latter study differs in the assumptions and the computational approach.

Table 7 *Relative changes of LW radiation fluxes at standard conditions, equal to the global averages, T = 288.6 K, e_a = 15.2 hPa, C = 0.671 (or C = 0 for clear sky), and with the indicated values of [CO₂] as calculated analytically and numerically by Equation (2). In parentheses are the values directly calculated by MODTRAN assuming midlatitude summer profile matching the above values of T and e_a, and altostratus clouds for the cloudy case.*

[CO₂] increase	Sky	Downwelling, L_D			Outgoing, L_D		
		ΔL_D	L_D mean*	% change	ΔL_O	L_D mean*	% change
From 300 to 420	Cloudy	1.93	382.4	0.5%	–1.18	235.1	–0.5%
		(0.31)	(374.1)	(0.1%)	(–1.00)	(238.0)	(–0.4%)
From 300 to 420	Clear	1.57	311.3	0.4%	–1.32	261.5	–0.5%
		(0.79)	(309.6)	(0.3%)	(–1.32)	(265.7)	(–0.5%)
From 300 to 800	Cloudy	5.63	384.2	1.5%	–3.45	234.0	–1.5%
		(0.63)	(374.3)	(0.2%)	(–2.89)	(237.0)	(–1.2%)
From 300 to 800	Clear	4.59	312.8	1.2%	–3.84	260.2	–1.5%
		(2.45)	(310.5)	(0.8%)	(–3.89)	(264.4)	(–1.5%)

* *Geometric mean.*

7. Discussion and Further Results

In light of the above results, we may revisit Lacis et al.'s (2010) statements quoted in the Introduction, leaving aside the fact they refer to imaginary world conditions. Specifically, even if we removed the CO_2 from the atmosphere, again there would be new emissions from volcanos and outgassing from the oceans, even if the biosphere was also removed. In the relatively recent glacial periods, covered by Vostok proxy data, the CO_2 concentration did not fall below 180 ppm. This value is perhaps the absolute low for the entire history of Earth. What would disappear from Earth in the imaginary-world case of CO_2 removal is not the greenhouse effect but life as we know it. For plants may not survive at CO_2 levels below 150 ppm (Gerhart and Ward, 2010) while without the photosynthesis performed by plants, the entire biosphere would collapse. On the opposite side, the increase in CO_2 is beneficial for plant growth. As recently reported and as a result of the recent increase, global greening is an "indisputable fact", and even its rate has increased slightly (Chen et al., 2024).

Furthermore, the notion of the effective temperature used by Lacis et al. is problematic because the temperature field of the Earth as a whole is not thermodynamically representable by a single temperature and the radiation from Earth deviates from a black body distribution, which is used to define the effective temperature (Essex et al., 2007). Moreover (and leaving aside this caveat), even the 10% of the current atmospheric value of water vapour for $T_S = T_E$, given in the quoted statement by Lacis et al., would produce a greenhouse effect and hence would imply the inequality $T_S \neq T_E$, thus leading to the absurd. That greenhouse effect would not be 10% or close to it, but closer to its current magnitude. Indeed, according to Brutsaert's equation (A12), for T_E/T_S = 255/288 (with 288 K being the current average temperature used by Brutsaert) and vapour pressure ratio of e_E/e_S = 0.1, the resulting emissivity ratio $\varepsilon_E/\varepsilon_S$ would be $(0.1 / (255/288))^{1/7} = 0.73$. An emissivity $e_E > 0$ means that we would again have the greenhouse effect produced by water vapour. (See also Table 5 and its discussion in Section 6.1.) And even in an "*icebound Earth state*", thermodynamics implies the presence of water vapour in the atmosphere, due to sublimation. Remarkably, though, geological evidence presented by Veizer (2005, 2011, 2012) suggests the presence of running water as far back as we have a record, up to 3.8 or even 4.2 billion years, despite the much smaller solar irradiance (the so-called faint young sun puzzle). All these imply that the argument is mistaken and so is the popular result that is being widely reproduced—now even by chatbots.

The distinction between feedbacks and forcings, also appearing in the quoted statements by Lacis et al., is problematic. Both H_2O and CO_2 have always been present on Earth and both are greenhouse gases, with the difference being that the former is much more abundant in the atmosphere and determinant for the greenhouse effect, as already demonstrated. Calling CO_2 forcing and H_2O feedback is like claiming that the tail wags the dog.

Water has more roles in climate than examined above. The greenhouse effect slows down the rate of Earth's cooling by LW radiation. However, Earth's surface cooling and its reaction, i.e., the atmosphere's warming, is not only due to LW radiation. According to Trenberth et al. (2009), the contribution of the LW radiation is 396 – 333 = 63 W/m^2, a value generally consistent with the results of this paper. This low value is due to the action of greenhouse gases, and, as we have seen, it is dominated by the presence of water vapour in the atmosphere. However, the greatest contribution to Earth's surface cooling, namely 80 W/m^2 (Trenberth et al., 2009; Koutsoyiannis, 2021), is due to the latent heat from evaporation (phase change of water from liquid to gaseous phase).

Surface cooling and atmosphere warming are reflected in the vertical profile of the net upgoing radiation flux, seen in Figure 25. Here the SW radiation was also considered, calculated by RRTM. The net radiation minus the absorbed SW radiation in the atmosphere is increasing with altitude. In the long term, as the energy is not stored in the atmosphere, the total heat transfer should be the same at all altitudes. The deficit of heat transfer in low altitudes is recovered by the transfer of sensible and latent heat, which warm the atmosphere. Figure 26 shows diagrammatically the contribution of each of these mechanisms to Earth's cooling and the atmosphere's warming.

Interestingly, heat exchange by evaporation (and hence the latent heat transfer from the Earth's surface to the atmosphere) is the Earth's natural locomotive, with the total energy involved in the hydrological cycle being 1290 ZJ/year, corresponding to an energy flux density of 80 W/m^2. Compared to human energy production, the total energy of the natural locomotive is 2100 times higher than that of humanity's locomotive (Koutsoyiannis, 2021). Notably, evaporation is a negative feedback of the climate as increased temperature causes evaporation to increase (cf. simplified equation (5) in Tegos et al., 2015). This increases the latent heat, which tends to lower the temperature, making evaporation a strong stabilizer for the climate (Harde, 2014, 2017; Clark, 2024, figure 32), a fact also reflected in Figure 6.

In addition to regulating the LW radiation flux and the latent heat flux, water vapour and clouds also regulate the SW radiation and Earth's albedo. Other properties of water, as listed in Koutsoyiannis (2021), are also determinants for climate. First is its unique property of existing on Earth in *all three phases* and in different formations, with spectacular differences among them in properties related to climate. Remarkable is its *abundance* on Earth, as only the part that is in turbulent motion amounts to 1.34×10^9 Gt (not counting quantities that are stored in the soil, ground and glaciers), 260 times larger than the total mass of the atmosphere. The *turbulent motion* of water, which is intrinsically uncertain, generates climatic phenomena at all scales, from large-scale coupled ocean-atmosphere fluctuations, such as the El Niño–Southern Oscillation (ENSO), Atlantic Multidecadal Oscillation (AMO) and Interdecadal Pacific Oscillation (IPO), to regional droughts and floods. The high specific heat (or *heat capacity*) of water, particularly in its liquid phase, combined with its abundance, makes water the climatic thermostat of the Earth, i.e., the element that determines the heat storage and through it the climate of the Earth. The high *specific latent heat* of vaporization (calculated from Equation (A5)) combined with the water occurrence on Earth in all three phases, makes water the thermodynamic regulator of climate. Finally, the fact that water is a universal solvent makes it an *elixir of life*, complementary to the CO_2 which is the other elixir of life, as through photosynthesis it is responsible for the organic matter on which life on Earth is based.

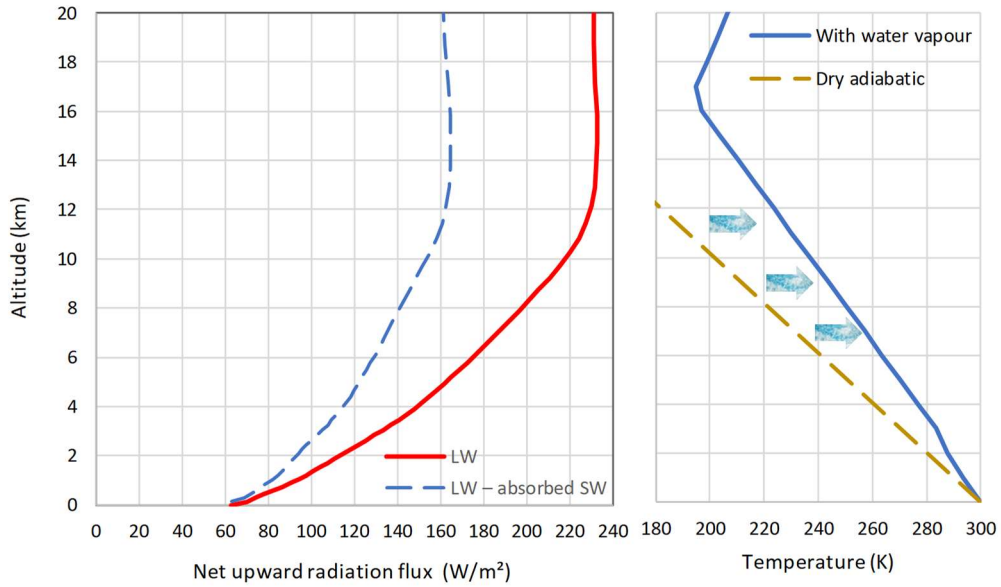

*Figure 25: **(left)** Vertical profile of net LW radiation flux for default conditions and standard tropical atmospheric profile (T = 299.7 K; $[CO_2]$ = 400 ppm; L_D = 369.26 W/m²; L_O = 298.49 W/m²), as calculated by MODTRAN, and its difference from the net SW profile, as calculated by the RRTM Earth's Energy Budget (https://climatemodels.uchicago.edu/rrtm/). **(right)** MODTRAN's standard tropical atmospheric profile of temperature, compared with the dry adiabatic profile (with a gradient of 9.8 K/km); the arrows indicated the heating of the atmosphere due to the latent heat released by condensation of water vapour, accumulated over elevation.*

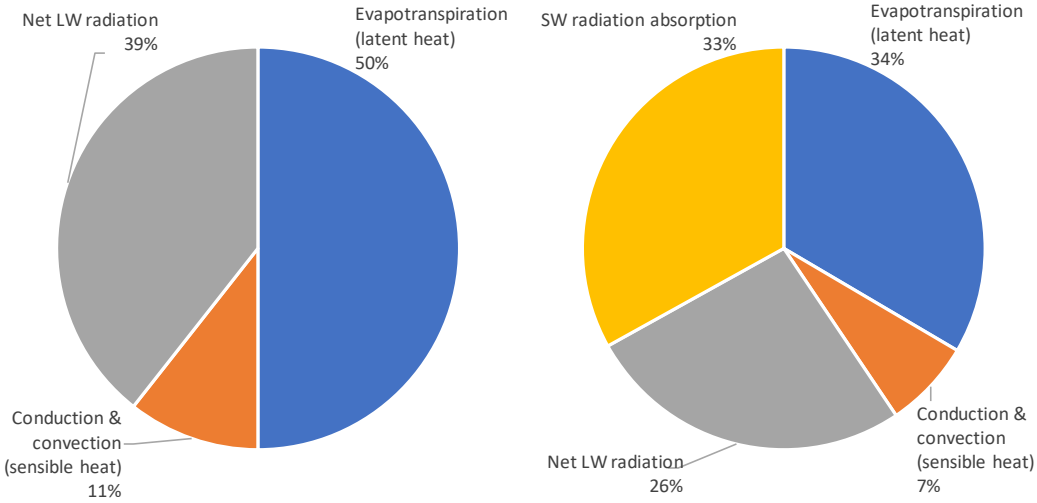

*Figure 26: Contribution of **(left)** the three mechanisms responsible for the cooling of Earth's surface and **(right)** the four mechanisms responsible for the warming of Earth's atmosphere, based on the global energy balance by Trenberth et al. (2009).*

Thus, the biosphere strongly depends on both CO_2 and H_2O. In particular, the presence of water determines the type and extent of ecosystems. In turn, the ecosystems affect climate at large through the carbon and oxygen cycles (where the vast majority of the CO_2 and O_2 emissions are products of life, through respiration and photosynthesis, respectively), and their contribution to the water cycle (transpiration) and in the carbon and energy cycles (photosynthesis). Humans, as part of the biosphere, also interact with water and climate, affecting them and being affected by them. Excluding human influences, the processes of the biosphere determine the vast majority (96%) of CO_2 emissions and partly, in the terrestrial part, the emission of H_2O by the transpiration process. And as Koutsoyiannis and Kundzewicz (2020), Koutsoyiannis et al. (2023) and

Koutsoyiannis (2024b) have shown, it is the relationship between temperature and biosphere that has determined the recent increase in the atmospheric [CO_2].

Considering all these facts, it is stunning that the whole "climate project", including climate modelling, is based on hypotheses and scenarios about human CO_2 emissions.

8. Conclusions

According to the calculations presented here and the depiction of the results in Figure 24, the contribution of CO_2 to the greenhouse effect is 4% – 5%. Human CO_2 emissions represent 4% of the total, which means that the total human contribution to the enhancement of the greenhouse effect is 0.16% to 0.20% —a negligible effect. Irrespective of the origin of the increase of [CO_2] in the last century, its contribution to the greenhouse effect is about 0.5%, below any threshold to make it observable. In contrast, water (including clouds) contributes to the atmospheric greenhouse effect by 87% to 95%. The physical background that makes water, in its different phases, to have the strongest impact on the radiation in the atmosphere and CO_2 to have a weak contribution are explained, with detailed spectroscopic calculations, by Harde (2013, 2014). In addition, 50% of Earth's cooling and atmosphere's warming is due to water (against 39% due to LW radiation, which again is dominated by water—Figure 26).

Common arguments trying to amplify the importance of human carbon emissions are that these accumulate in the atmosphere and that they cause temperature to rise. The former argument is mistaken as the atmosphere does not have any mechanism to separate the incoming CO_2 according to its origin, and to accumulate that part that comes from humans. Also, the second argument has been refuted by showing, using both paleoclimatic proxies and modern instrumental CO_2 and temperature time series, that temperature changes precede CO_2 changes and thus the CO_2 increase cannot be a cause of the temperature increase (Koutsoyiannis and Kundzewicz, 2020; Koutsoyiannis et al., 2022a,b, 2023; Koutsoyiannis, 2024a).

Given these recent developments, the case of the magnified importance of CO_2, and particularly the human emissions thereof, appears to be a historical accident in scientific terms, that was exploited in non-scientific terms. If we return to science, the proper path is to improve hydrology and stochastics to better understand and model climate. For climate is mostly hydrology in terms of its driving physical mechanisms (as articulated here) and mostly stochastics in terms of its proper mathematical representation (as implied by its very definition; cf. Koutsoyiannis 2021, 2023).

Appendix A: Quantification of Greenhouse Gases and of Longwave Radiation

The typical quantification of the abundance of a specific gas X in a gas mixture is given by the simple metric in Equation (1). Another metric is provided by the mass fraction:

$$q_X = \frac{M_X}{M_{\mathrm{TOT}}} = \frac{\rho_X}{\rho_{\mathrm{TOT}}} = \frac{m_X n_X}{m_{\mathrm{TOT}} n_{\mathrm{TOT}}} = \frac{m_X}{m_{\mathrm{TOT}}}[X] \tag{A1}$$

where M_X and M_{TOT} are the mass of the gas and the total mass of all constituents at a specified volume V, ρ_X and ρ_{TOT} are the respective densities ($\rho_X = M_X/V, \rho_{\mathrm{TOT}} = M_{\mathrm{TOT}}/V$), and m_X and m_{TOT} are respective molar masses (in units of mass per mole).

The partial pressure of X, p_X, provides another quantification. Under the ideal gas law and the above equation, we find:

$$p_X = \frac{\rho_X R_* T}{m_X} = \frac{\rho_{\mathrm{TOT}} R_* T}{m_{\mathrm{TOT}}}[X] = p_{\mathrm{TOT}}[X] \tag{A2}$$

where $R_* = 8.314$ J K^{-1} mol^{-1} is the universal gas constant and T is the temperature.

As an example, we consider the atmosphere in standard conditions at mean sea level, i.e., $p \equiv p_{\mathrm{TOT}} = 1013.25$ hPa, T = 15 °C = 288.15 K, $\rho_{\mathrm{TOT}} = 1.225$ kg/m^3. The molar mass of the mixture is $m_{\mathrm{TOT}} = \rho_{\mathrm{TOT}} R_* T / p_{\mathrm{TOT}} = 28.96$ kg/kmol. Considering CO_2 as the specific gas of interest, with molar mass $m_{\mathrm{CO_2}} = 44.01$ kg/kmol, at concentration [CO_2] = 400 ppm, we find that $q_{\mathrm{CO_2}} = (m_X / m_{\mathrm{TOT}})\,[X] = 607.8$ ppm and $p_{\mathrm{CO_2}} = p_{\mathrm{TOT}}[X] = 0.4$ hPa.

For the water vapour in the atmosphere, whose partial pressure by convention is denoted as e_{a}, the concentration varies substantially in space and time. The mass fraction, known as specific humidity, is found, after algebraic manipulations, to be:

$$q = \frac{\varepsilon e_{\mathrm{a}}}{p - (1-\varepsilon) e_{\mathrm{a}}} \tag{A3}$$

where ε is the ratio of the molecular mass of water to that of the mixture of gases in the dry air, i.e., ε = 18.016/28.966 = 0.622. As an example, for a typical value of $e_{\mathrm{a}} = 15$ hPa (see Section 6.2) and standard atmospheric conditions as above, we find q = 9.3‰ and [H_2O] = 14.9‰ (almost 40 times higher than in the above typical example of CO_2).

The water vapour pressure has a thermodynamic upper limit, the saturation water vapour pressure, which is a function of the temperature, T:

$$e(T) = e_0 \exp\left(\frac{\alpha}{R T_0}\left(1 - \frac{T_0}{T}\right)\right)\left(\frac{T_0}{T}\right)^{(c_{\mathrm{L}} - c_p)/R} \tag{A4}$$

where (T_0, e_0) are the coordinates of the triple point of water ($T_0 = 273.16$ K, $e_0 = 6.11657$ hPa), $R := R_*/m$ is the specific gas constant of water vapour ($R = 461.5$ J kg^{-1}K^{-1}), c_p is the specific heat at constant pressure of the water vapour ($c_p = 1884.4$ J kg^{-1} K^{-1}), c_{L} is the specific heat of the liquid water ($c_L = 4219.9$ J kg^{-1} K^{-1}), and $\alpha := \xi R/k = \xi N_{\mathrm{A}}$, with k the Boltzmann's constant, and ξ is the amount of energy required for a molecule to move from the liquid to gaseous phase. The parameter α is related to the latent heat of vaporization, Λ:

$$\alpha = \Lambda_0 + (c_L - c_p) T_0 = \Lambda + (c_L - c_p) T \tag{A5}$$

which is valid for any T, where at the triple point $\Lambda_0 = 2.501 \times 10^6$ J kg^{-1}. By substitution of the various constants in (A4), the following form of the equation is derived (first presented in Koutsoyiannis, 2012):

$$e(T_{\mathrm{a}}) = e_0 \exp\left(24.921\left(1 - \frac{T_0}{T_{\mathrm{a}}}\right)\right)\left(\frac{T_0}{T_{\mathrm{a}}}\right)^{5.06}, \quad T_0 = 273.16\ \mathrm{K}, e_0 = 6.11657\ \mathrm{hPa} \tag{A6}$$

This is a very accurate form of the celebrated Clausius-Clapeyron equation, which was recently rederived in a pure stochastic context by maximizing the entropy, i.e., the uncertainty, in a single water molecule (Koutsoyiannis, 2014, 2023). Notably, the maximization of uncertainty at the microscopic level yields a law that at the macroscopic level is nearly deterministic.

For completeness, we also produce the equation for the saturation water pressure over ice. In this case, it suffices to replace in Equation (A4) the specific heat of liquid water c_{L} with that of ice, c_{I}, and the latent heat of vaporization with that of sublimation, resulting in a constant α_{I} to substitute for α. Following Ambaum (2020), we adopt the value $c_{\mathrm{I}} = 2097$ J kg^{-1} K^{-1} and hence $(c_{\mathrm{I}} - c_p)/R = 0.461$. Optimizing the average relative square error from benchmark values provided by Murphy and Koop (2005; Appendix C) for temperatures 150 to 273.16 K, we find $\alpha_{\mathrm{I}}/RT_0 = 22.812$. Hence, the equation for the saturation water pressure over ice becomes:

$$e_{\mathrm{I}}(T_{\mathrm{a}}) = e_0 \exp\left(22.812\left(1-\frac{T_0}{T_{\mathrm{a}}}\right)\right)\left(\frac{T_0}{T_{\mathrm{a}}}\right)^{0.461}, \quad T_0 = 273.16\ \mathrm{K}, e_0 = 6.11657\ \mathrm{hPa} \tag{A7}$$

A state in which the vapour pressure e_{a} is lower than the saturation pressure $e(T)$ is characterized by the relative humidity:

$$U := \frac{e_a}{e(T)} = \frac{e(T_{\mathrm{d}})}{e(T)} \tag{A8}$$

which serves as a formal definition of both the relative humidity U and the dew point T_{d}.

The longwave radiation flux, L, from a body (measured as energy per unit time and unit area, typically $\mathrm{W/m^2}$) at temperature T (measured in kelvins) is described by the Stefan-Boltzmann law:

$$L = \varepsilon\sigma T^4 \tag{A9}$$

where ε is the emissivity of the body (dimensionless, with $\varepsilon = 1$ for a black body radiator) and σ is the Stefan–Boltzmann constant, a fixed physical constant that is related to other fundamental physical and mathematical constants by

$$\sigma = \frac{2\pi^5 k^4}{15c^2h^3} = 5.67\times10^{-8}\ \mathrm{W\,m^{-2}\,K^{-4}} \tag{A10}$$

Here, π is the ratio of a circle's circumference to its diameter, k is the Boltzmann's constant, h is the Planck's constant, and c is the speed of light in vacuum.

At the Earth's surface, the three LW radiation fluxes of interest are: (a) L_{s}, emitted by the surface (solid or liquid) directed upward, (b) L_{D}, emitted by the atmosphere directed downward, and (c) L_{n}, the net emission. These are given as:

$$L_{\mathrm{s}} = \varepsilon_{\mathrm{s}}\sigma T_{\mathrm{s}}^4, \qquad L_{\mathrm{D}} = \varepsilon_{\mathrm{a}}\sigma T_{\mathrm{a}}^4, \qquad L_{\mathrm{n}} = L_{\mathrm{s}} - L_{\mathrm{D}} \tag{A11}$$

where in the last equation a minor term of reflected upward longwave radiation has been neglected. The temperature of the surface, T_{s}, is well defined and the emissivity ε_{s} is close to 1, usually taken $\varepsilon_{\mathrm{s}} = 0.97$. However, in the atmosphere the temperature varies substantially and the quantity L_{D} is the integration of the radiation process across the entire atmosphere.

The theoretical basis for such integration is described by Goody (1964). Based on this theoretical basis and some assumptions on the atmospheric profiles (nearly standard atmosphere), Brutsaert (1975) was able to express analytically (by integration) the atmospheric radiation L_{a} near the surface for clear sky, and eventually find the effective emissivity as a function of the atmospheric temperature, T_{a}, taken at a level near Earth's surface, and the partial pressure of water vapour, e_{a}, taken at the same level:

$$\varepsilon_{\mathrm{a}} = 1.24\left(\frac{e_{\mathrm{a}}/\mathrm{hPa}}{T_{\mathrm{a}}/\mathrm{K}}\right)^{1/7} \tag{A12}$$

He also proposed a simplification by fixing T_{a} to the average Earth's temperature near the surface, i.e. to 288 K, whence Equation (A12) becomes

$$\varepsilon_{\mathrm{a}} = 0.553(e_{\mathrm{a}}/\mathrm{hPa})^{1/7} \tag{A13}$$

A modification of the Brutsaert's Equation (A12) was proposed by Prata (1996), which is expressed as:

$$\varepsilon_\mathrm{a} = 1 - (1 + w)\exp\left(-\sqrt{1.2 + 3.0w}\right), \qquad w := 46.5\frac{e_\mathrm{a}/\mathrm{hPa}}{T_\mathrm{a}/\mathrm{K}} \tag{A14}$$

with w representing the atmospheric water content (most commonly known with the misnomer 'precipitable water'), found by linear regression on radiosonde data and expressed in cm. We may observe that for $e_\mathrm{a} = 0$, Brutsaert's equation (A12) results in zero emissivity, while Prata's Equation (A14) has a nonzero minimum of $\varepsilon_\mathrm{a} = 0.67$ and, in this way, it describes the non-condensing greenhouse gas contribution to emissivity.

Decades earlier, empirical relationships of the same type (and with nonzero minimum) had been proposed, among which the earliest, most celebrated and most popular is that by Brunt (1932, 1934):

$$\varepsilon_\mathrm{a} = 0.526 + 0.065\sqrt{e_\mathrm{a}/\mathrm{hPa}} \tag{A15}$$

Furthermore, Brunt (1954), using several data sets, fitted the mathematical expression

$$\varepsilon_\mathrm{a} = a + b\sqrt{e_\mathrm{a}/\mathrm{hPa}} \tag{A16}$$

and found different values of the coefficients a and b for each data set. An average fitting for all cases is:

$$\varepsilon_\mathrm{a} = 0.44 + 0.08\sqrt{e_\mathrm{a}/\mathrm{hPa}} \tag{A17}$$

With Penman's (1948) celebrated paper on evaporation, this quantification became an essential part of hydrological practice in calculating evaporation. Essentially, Penman used Brunt's Equation (A17), also assuming that $T_\mathrm{s} = T_\mathrm{a}$ and $\varepsilon_\mathrm{s} = 1$. Indeed, it can be readily seen that Penman's (1948) original equation (numbered (7) in his paper), which for clear sky conditions reads

$$\frac{L_\mathrm{n}}{\sigma T_\mathrm{a}^4} = 0.56 - 0.08\sqrt{e_\mathrm{a}/\mathrm{hPa}} \tag{A18}$$

is a direct result of Brunt's Equation (A17) and these assumptions, even though Penman (1948) did not make a distinction between the two components seen in Equation (A11).

Later Penman's equation was complemented by Monteith (1965) to estimate the water requirements of crops, thus shaping what has been called the Penman-Monteith method. This became a standard of the Food and Industry Organization (FAO), initially in the version by Doorenbos and Pruitt (1977) and later in the version by Allen et al. (1998). In both versions, the downwelling longwave radiation (again assuming that $T_\mathrm{s} = T_\mathrm{a}$ and $\varepsilon_\mathrm{s} = 1$) is calculated as

$$\varepsilon_\mathrm{a} = 0.66 + 0.044\sqrt{e_\mathrm{a}/\mathrm{hPa}} \tag{A19}$$

Subsequently, a large variety of similar empirical relationships were proposed by several researchers, critical reviews of which can be found in Carmona et al. (2014), Guo et al. (2019) and Wong et al. (2023), to mention the most recent.

Appendix B: MODTRAN locality profiles

MODTRAN implements five different locality profiles, which differ in their temperature, H_2O and O_3 profiles. The profiles most relevant to this study are depicted Figure A1[12]. By comparison with zonal temperature distributions analogous to that in Figure 4, but separately for summer and

[12] Additional information can be found in "The 6 model atmospheres in MODTRAN", accessed 19 February 2024, http://modtran.spectral.com/static/modtran6/html/help_atmosphere_model.html

winter, we infer that the tropical profile corresponds roughly to the equator, but is representative for the entire torrid zone (between 23.4° N or S), the midlatitude profile corresponds to a latitude at about 45° N or S, and the subarctic profile at about the latitude of polar circles (66.6° N or S). In addition, MODTRAN includes the 1976 U.S. Standard Atmosphere temperature profile, which provides an effective median for the set of locality profiles; this was not used in this study.

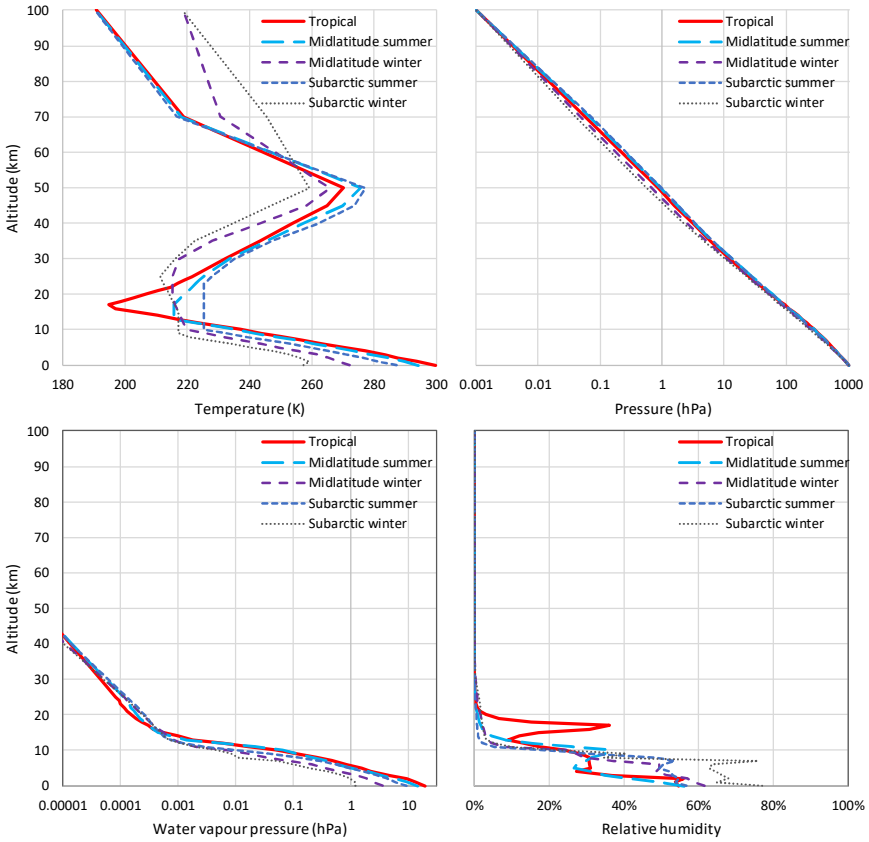

Figure A1: Standard profiles of the indicated variables used in MODTRAN.

Figure A2 depicts a characteristic example of MODTRAN output profiles upward, downward and net LW radiation flux across the atmosphere for the tropical profile and default settings. Above the level of 20 km, the downward LW radiation is very low and the upward LW radiation, total or net, is almost constant.

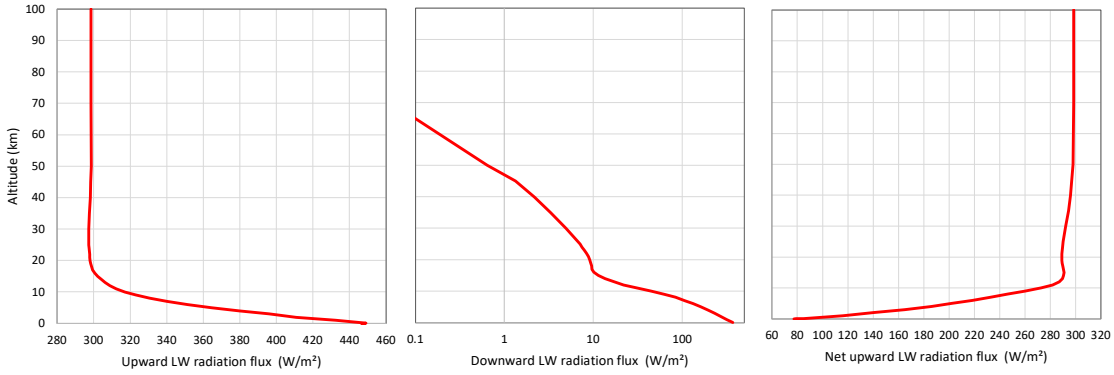

Figure A2: Profiles of the indicated variables resulting from MODTRAN for the tropical profile and default settings.

Supplementary Information

Earlier review comments from other journals, which did not accept the paper, are posted as Supplementary Information, along with the replies to comments and exchanges with editorial offices (see: https://scienceofclimatechange.org/wp-content/uploads/Dog_and_Tail_SI_ocred.pdf).

Funding

This research received no funding but was conducted out of scientific curiosity.

Guest-Editor: H. Harde; Reviewers: anonymous.

Data Availability Statement

This research uses no new data. The data sets used have been retrieved from the sources described in detail in the text.

Conflicts of Interest

I declare that I have no competing financial interests or personal relationships that could have appeared to influence the work reported in this paper.

Acknowledgements

I am grateful to the colleagues and organizations who have put their huge data sets online along with the data processing and computational systems they have developed. These include the CERES data, the ERA5 and NCEP/NCAR Reanalyses, the CLIMEXP data and software platform, and the MODTRAN and RRTM software systems.

I thank the Editor Hermann Harde and an anonymous reviewer for their comments and the favourable assessment of my paper.

I thank Richard Cina for his constructive suggestions on the first draft of the paper and Ariane Loening for editorial corrections. I am grateful to William Happer for his encouragement and his helpful comments on an earlier draft of the paper.

I thank an anonymous reviewer of a predecessor paper (Koutsoyiannis and Vournas, 2024), whose critical comments made it necessary to delve into the topic examined in the present paper. The brief reply to those review comments was not included in the predecessor paper in order not to distract its focus. Yet it constituted the springboard to produce this paper.

I acknowledge three rejections of this paper. The first was by *Hydrological Sciences Journal* with a unanimous decision of all five editors (Attilio Castellarin, Stacey Archfield, Aldo Fiori, Riddhi Singh, Konstantinos Soulis) without review. The second by the MDPI *Hydrology* by a decision by the Editor-in-Chief Ezio Todini, based on a unanimous recommendation for rejection by four anonymous reviewers. The third was by an anonymous editor of *Hydroecology and Engineering*. The latter journal's staff invited the paper, and before its submission (but after its posting as a preprint) informed me that they "believe in the importance of diverse perspectives in scientific discourse". After its submission, they initially accepted it with major revisions. After I addressed or rebutted the review comments, they eventually rejected it. As I believe that the prehistory of rejections is very informative and confirms the assertions I made in the Introduction, I have compiled all the review materials and editorial exchanges into a lengthy document published as Supplementary Information.

References

Allen RG, Pereira LS, Raes D, Smith M. 1998: *Crop Evapotranspiration – Guidelines for Computing Crop Water Requirements*. FAO Irrigation and Drainage Paper 56, Food and Agriculture Organization of the United Nations, Rome, https://www.fao.org/3/X0490E/x0490e00.htm

(accessed 25 August 2023).

Ambaum MHP, 2020: *Accurate, simple equation for saturated vapor pressure over water and ice,* Q. J. R. Meteorol. Soc., 146, 4252–4258. doi:10.1002/qj.3899

Berk A, Bernstein LS, Robertson DC, 1987: *MODTRAN: A Moderate Resolution Model for LOWTRAN*, Scientific Report No. 1; Air Force Geophysics Laboratory, Air Force Systems Command, United States Air Force: Hanscom Air Force Base, Massachusetts, USA, https://apps.dtic.mil/sti/pdfs/ADA185384.pdf (accessed 19 February 2024).

Berk A, Acharya PK, Bernstein LS, Anderson GP, Lewis P, Chetwynd JH, Hoke ML, 2008: *Band model method for modeling atmospheric propagation at arbitrarily fine spectral resolution*, U.S. Patent #7433806.

Berk A, Conforti P, Kennett R, Perkins T, Hawes F, van den Bosch J. 2014: *MODTRAN6: A Major Upgrade of the MODTRAN Radiative Transfer Code*, Proc. SPIE, 9088, 90880H. doi:10.1117/12.2050433.

Biermann F, Abbott K, Andresen S, Bäckstrand K, Bernstein S, Betsill MM, Bulkeley H, Cashore B, Clapp J, Folke C, et al., 2012: *Navigating the anthropocene: improving earth system governance*, Science, 335, 1306–1307.

Brooks FA, 1952: *Atmospheric radiation and its reflection from the ground*, J. Atmos. Sci., 9, 41–52.

Brunt D. 1932: *Notes on radiation in the atmosphere*, I. Q. J. R. Meteorol. Soc., 58, 389–420.

Brunt D, 1934: *Physical and Dynamical Meteorology*, Cambridge University Press: Cambridge, UK,; 411 pp., https://archive.org/details/in.ernet.dli.2015.215092 (accessed 25 August 2023).

Brutsaert W, 1975: *On a derivable formula for long-wave radiation from clear skies*, Water Resour. Res., 11, 742–744.

Brutsaert W, 1991: *Evaporation into the Atmosphere: Theory, History and Applications*, Springer Science & Business Media: Dordrecht, Netherlands,; 299 pp.

Carmona F, Rivas R, Caselles V, 2014: *Estimation of daytime downward longwave radiation under clear and cloudy skies conditions over a sub-humid region*, Theor. Appl. Climatol., 115, 281–295.

CERES, 2021: *CERES_EBAF_Ed4.1 Data Quality Summary*, Version 3 (Updated 12/9/2021). (accessed 15 February 2024).
https://ceres.larc.nasa.gov/documents/DQ_summaries/CERES_EBAF_Ed4.1_DQS.pdf

CERES, 2021: *CERES_SSF1deg_Hour/Day/Month_Ed4A Data Quality Summary*, Version 2 (Updated 8/4/2023), (accessed 15 February 2024).
https://ceres.larc.nasa.gov/documents/DQ_summaries/CERES_SSF1deg_Ed4A_DQS.pdf

Chen X, Chen T, He B, Liu S, Zhou S, Shi T, 2024: *The global greening continues despite increased drought stress since 2000*, Glob. Ecol. Conserv., 49, e02791.

Clark R, 2013a: *A dynamic, coupled thermal reservoir approach to atmospheric energy transfer Part I: Concepts*, Energy and Environment, 24 (3-4), 319-340, doi: 10.1260/0958-305X.24.3-4.319.

Clark R, 2013b: *A dynamic, coupled thermal reservoir approach to atmospheric energy transfer Part II: Applications*, Energy and Environment, 24 (3-4), 341-359, doi: 10.1260/0958-305X.24.3-4.341.

Clark R, 2024: *A Nobel Prize for Climate Modeling*, Science of Climate Change, 4 (1), 1-73, doi: 10.53234/scc202404/17.

de Lange CA, Ferguson JD, Happer W, van Wijngaarden WA, 2022: *Nitrous oxide and climate*,

arXiv, arXiv:2211.15780, https://arxiv.org/abs/2211.15780 (accessed 25 August 2023).

Dingman SL, 1994: *Physical Hydrology*, Prentice Hall, Upper Saddle River, New Jersey, USA.

Doelling DR, Loeb NG, Keyes DF, Nordeen ML, Morstad D, Nguyen, C.; Wielicki, B.A.; Young, D.F.; Sun, M, 2013: *Geostationary enhanced temporal interpolation for CERES flux products*, J. Atmos. Ocean. Technol., 30, 1072–1090, doi: 10.1175/JTECH-D-12-00136.1.

Doelling DR, Sun M, Nguyen LT, Nordeen ML, Haney CO, Keyes DF, Mlynczak PE, 2016: *Advances in geostationary-derived longwave fluxes for the CERES synoptic (SYN1deg) product*, J. Atmos. Ocean. Technol., 33, 503–521, doi: 10.1175/JTECH-D-15-0147.1.

Dooge JC, 1986: *Looking for hydrologic laws*, Water Resour. Res., 22, 46S–58S.

Doorenbos J, Pruitt WO, 1977: *Guidelines for Predicting Crop Water Requirements*, FAO Irrigation and Drainage Paper 24, Food and Agriculture Organization of the United Nations, Rome, https://dokumen.tips/download/link/fao-irrigation-and-drainage-paper-24.html (accessed 25 August 2023).

Eschenbach W, 2010: *The thunderstorm thermostat hypothesis*. Energy and Environment, 21 (4), 201-200, doi: 10.1260/0958-305X.21.4.201.

Essex C, McKitrick R, Andresen B, 2007: *Does a global temperature exist?* J. Non-Equilibrium Thermodynamics, 32 (1), 1-27, doi: 10.1515/JNETDY.2007.001.

Gerhart LM, Ward JK, 2010: *Plant responses to low [CO2] of the past*, New Phytol., 188, 674–695.

Goody RM, 1964: *Atmospheric Radiation*, Oxford University Press, Oxford, UK; New York, NY, USA, 436 pp.

Guo Y, Cheng J, Liang S, 2019: *Comprehensive assessment of parameterization methods for estimating clear-sky surface downward longwave radiation*, Theor. Appl. Climatol., 135, 1045–1058.

Harde H, 2013: *Radiation and heat transfer in the atmosphere: a comprehensive approach on a molecular basis*, International Journal of Atmospheric Sciences, 2013(1), http://dx.doi.org/10.1155/2013/503727.

Harde H, 2014: *Advanced two-layer climate model for the assessment of global warming by CO2*, Open Journal of Atmospheric and Climate Change, 1 (3), https://web.archive.org/web/20160429061756/ http://www.scipublish.com/journals/ACC/papers/download/3001-846.pdf.

Harde H, 2017: *Radiation transfer calculations and assessment of global warming by CO2*, Int. J. Atmos. Sci., 9251034, 1-30, https://doi.org/10.1155/2017/9251034.

Harde H, 2022: *How much CO_2 and the sun contribute to global warming: Comparison of simulated temperature trends with last century observations,* Science of Climate Change, 2(2), 105-133, https://doi.org/10.53234/scc202206/10.

Howe N, 2020: *'Stick to the science': when science gets political,* Nature, doi: 10.1038/d41586-020-03067-w.

Jacobs JD, 1978: *Radiation climate of Broughton Island*, In Energy Budget Studies in Relation to Fast-Ice Breakup Processes in Davis Strait, Barry RG, Jacobs JD, Eds.; Inst. of Arctic and Alp. Res. Occas. Paper no. 26; University of Colorado: Boulder, USA, 105–120, https://www.colorado.edu/instaar/node/963 (accessed 13 February 2024).

Kato S, Rose FG, Rutan DA, Thorsen TE, Loeb NG, Doelling DR, Huang X, Smith WL, Su W, Ham S-H, 2018: *Surface irradiances of Edition 4.0 Clouds and the Earth's Radiant Energy System (CERES) Energy Balanced and Filled (EBAF) data product*, J. Clim., 31, 4501–4527, doi: 10.1175/JCLI-D-17-0523.1.

Koll, DDB, Cronin, TW, 2018: *Earth's outgoing longwave radiation linear due to H_2O greenhouse effect*, PNAS, 115 (41), 10293-10298, doi: 10.1073/pnas.1809868115.

Koutsoyiannis D, 2012: *Clausius-Clapeyron equation and saturation vapor pressure: simple theory reconciled with practice*, Eur. J. Phys., 33, 295–305. doi:10.1088/0143-0807/33/2/295

Koutsoyiannis D, 2014: *Entropy: from thermodynamics to hydrology*, Entropy, 16, 1287–1314, doi: 10.3390/e16031287.

Koutsoyiannis D, 2020a: *Revisiting the global hydrological cycle: is it intensifying?*, Hydrol. Earth Syst. Sci., 24, 3899–3932, doi: 10.5194/hess-24-3899-2020.

Koutsoyiannis D, 2020b: *Rebuttal to review comments on "Revisiting global hydrological cycle: Is it intensifying?"*, Hydrol. Earth Syst. Sci. Discuss., doi: 10.5194/hess-2020-120-AC1, https://hess.copernicus.org/preprints/hess-2020-120/hess-2020-120-AC1-supplement.pdf (accessed 2022-02-13).

Koutsoyiannis D, 2021: *Rethinking climate, climate change, and their relationship with water*, Water, 13, 849, doi: 10.3390/w13060849.

Koutsoyiannis D, 2023: *Stochastics of Hydroclimatic Extremes – A Cool Look at Risk*, Edition 3, Kallipos Open Academic Editions, Athens, 391 pp, doi: 10.57713/kallipos-1.

Koutsoyiannis D, 2024a: *Stochastic assessment of temperature – CO_2 causal relationship in climate from the Phanerozoic through modern times,* Mathematical Biosciences and Engineering, 21 (7), 6560–6602, doi: 10.3934/mbe.2024287.

Koutsoyiannis D, 2024b: *Refined reservoir routing (RRR) and its application to atmospheric carbon dioxide balance*, Water, 16 (17), 2402, doi: 10.3390/w16172402.

Koutsoyiannis D, Kundzewicz ZW, 2020: *Atmospheric temperature and CO_2: Hen-or-egg causality?*, Sci, 2, 72, doi:10.3390/sci2040077.

Koutsoyiannis D, Mamassis N, 2021: *From mythology to science: the development of scientific hydrological concepts in the Greek antiquity and its relevance to modern hydrology*, Hydrology and Earth System Sciences, 25, 2419–2444, doi: 10.5194/hess-25-2419-2021.

Koutsoyiannis D, Onof C, Christofides A, Kundzewicz ZW, 2022a: *Revisiting causality using stochastics: 1. Theory*, Proc. R. Soc. A, 478, 20210835, doi: 10.1098/rspa.2021.0835.

Koutsoyiannis D, Onof C, Christofides A, Kundzewicz ZW, 2022b: *Revisiting causality using stochastics: 2. Applications*, Proc. R. Soc. A, 478, 20210836, doi: 10.1098/rspa.2021.0836.

Koutsoyiannis D, Onof C, Kundzewicz ZW, Christofides A, 2023: *On hens, eggs, temperatures and CO2: Causal links in earth's atmosphere*, Sci, 5, 35, doi:10.3390/sci5030035.

Koutsoyiannis D., Vournas C, 2024: *Revisiting the greenhouse effect—a hydrological perspective*, Hydrol. Sci. J., 69, 151–164, doi: 10.1080/02626667.2023.2287047.

Lacis AA, Schmidt GA, Rind D, Ruedy RA, 2010: *Atmospheric CO2: Principal control knob governing Earth's temperature*, Science, 330, 356–359.

Lhomme JP, Vacher JJ, Rocheteau A, 2007: *Estimating downward long-wave radiation on the Andean Altiplano*, Agric. For. Meteorol., 145, 139–148.

Li X, Peachey B, Maeda N, 2024: *Global warming and anthropogenic emissions of water vapor*, Langmuir, 40 (14), 7701-7709.

Loeb NG, Doelling DR, Wang H, Su W, Nguyen C, Corbett JG, Liang L, Mitrescu C, Rose FG, Kato S, 2018: *Clouds and the Earth's Radiant Energy System (CERES) Energy Balanced and Filled (EBAF) Top-of-Atmosphere (TOA) Edition-4.0 Data Product*, J. Clim., 31, 895–918, doi: 10.1175/JCLI-D-17-0208.1.

Lupia A, 2023: *Political endorsements can affect scientific credibility*, Nature, 615, 590-591, doi:

10.1038/d41586-023-00799-3.

Masson-Delmotte V, Zhai P, Pirani A, Connors SL, Péan C, Berger S, Caud N, Chen Y, Goldfarb L, Gomis MI, et al. (Eds.), 2021: IPCC, *Climate Change 2021: The Physical Science Basis*, Contribution of Working Group I to the Sixth Assessment Report of the Intergovernmental Panel on Climate Change, Cambridge University Press, Cambridge, UK; New York, NY, USA, 2391 pp.

Miskolczi F, 2023: *Greenhouse gas theories and observed radiative properties of the Earth's atmosphere*, Sci. Clim. Change, 3, 232–289, doi: 10.53234/scc202304/05.

Monteith JL, 1965: *Evaporation and environment*, Symposia of the Society for Experimental Biology, 19, 205–234.

Murphy, D.M.; Koop, T, 2005: *Review of the vapor pressures of ice and supercooled water for atmospheric applications*, Q. J. R. Meteorol. Soc., 131, 1539–1565.

Nature Editorial, 2023: S*hould Nature endorse political candidates? Yes — when the occasion demands it*, Nature, 615, 561, doi: 10.1038/d41586-023-00789-5.

Nikolov N., Zeller K, 2017: *New insights on the physical nature of the atmospheric greenhouse effect deduced from an empirical planetary temperature*, Model. Environ. Pollut. Climate Change, 1, 1000112, doi: 10.4172/2573-458X.1000112.

Peachey B, 2006: *Mitigating human enhanced water emission impacts on climate change*, In 2006 IEEE EIC Climate Change Conference, doi: 10.1109/EICCCC.2006.277221.

Penman HL, 1948: *Natural evaporation from open water, bare soil and grass*, Proc. R. Soc. Lond. A Math. Phys. Eng. Sci., 193, 120–145.

Philipona R, Kräuchi A, Brocard E, 2012: *Solar and thermal radiation profiles and radiative forcing measured through the atmosphere*, Geophys. Res. Lett., 39, L13806, doi: 10.1029/2012GL052087.

Prata AJ, 1996: *A new long-wave formula for estimating downward clear-sky radiation at the surface*, Q. J. R. Meteorol. Soc., 122, 1127–1151.

Salby ML, 2012: *Physics of the Atmosphere and Climate*, Cambridge University Press, New York, NY, USA.

Schmidt GA, Ruedy RA, Miller RL, Lacis AA, 2010: *Attribution of the present-day total greenhouse effect*, J. Geophys. Res., 115, D20106.

Searle JR, 1984: *Minds, Brains and Science*, Harvard University Press: Cambridge, MA, USA.

Sherwood SC, Dixit V, Salomez C, 2018: *The global warming potential of near-surface emitted water vapor*, Environmental Research Letters, 13 (10), 104006.

Tegos A, Malamos, N, Koutsoyiannis D, 2015: A parsimonious regional parametric evapotranspiration model based on a simplification of the Penman–Monteith formula, Journal of Hydrology, 524, 708-717, doi: 10.1016/j.jhydrol.2015.03.024.

Trenberth KE, Fasullo JT, Kiehl J, 2009: *Earth's global energy budget*, Bull. Am. Meteorol. Soc., 90, 311–324, doi:10.1175/2008BAMS2634.1.

UNESCO (United Nations Educational, Scientific and Cultural Organization) 1964: *Final Report, International Hydrological Decade, Intergovernmental Meeting of Experts*, UNESCO/NS/188; UNESCO House: Paris, https://unesdoc.unesco.org/images/0001/000170/017099EB.pdf (accessed 15 February 2024).

van Wijngaarden WA, Happer W, 2020: *Dependence of Earth's thermal radiation on five most abundant greenhouse gases*, arXiv, arXiv:2006.03098, https://arxiv.org/abs/2006.03098 (accessed 25 August 2023).

Veizer J, 2005: *Celestial climate driver: a perspective from four billion years of the carbon cycle*,

Geoscience Canada, 32, 13-28.

Veizer J, 2011: *The role of water in the fate of carbon dioxide: implications for the climate system*, In 43rd Int. Seminar on Nuclear War and Planetary Emergencies, Ragaini R (Ed.). World Scientific, 313-327, doi: 10.1142/8232.

Veizer J, 2012: *Planetary temperatures/climate across geological time scales*, In International Seminar on Nuclear War and Planetary Emergencies—44th Session: The Role of Science in the Third Millennium, 287-288.

Wielicki BA, Barkstrom BR, Harrison EF, Lee III RB, Smith GL, Cooper JE, 1996: *Clouds and the Earth's Radiant Energy System (CERES): An Earth observing system experiment*, Bull. Amer. Meteor. Soc., 77, 853-868, doi: 10.1175/1520-0477(1996)077<0853:CATERE>2.0.CO;2

Wong RY, Tso CY, Jeong SY, Fu SC, Chao CY, 2023: *Critical sky temperatures for passive radiative cooling*, Renewable Energy, 211, 214-226.

Zhang FJ, 2023: *Political endorsement by Nature and trust in scientific expertise during COVID-19*, Nature Human Behaviour, 7(5), 696-706, doi: 10.1038/s41562-023-01537-5.